# NASA CONTRACTOR
# REPORT

## CASE FILE
## COPY

# FINITE ELEMENT ANALYSIS AND COMPUTER GRAPHICS VISUALIZATION OF FLOW AROUND PITCHING AND PLUNGING AIRFOILS

*by Theodore Bratanow and Akin Ecer*

*Prepared by*
UNIVERSITY OF WISCONSIN-MILWAUKEE
Milwaukee, Wis.
*for Langley Research Center*

| 1. Report No.<br>NASA CR-2249 | 2. Government Accession No. | 3. Recipient's Catalog No. |
|---|---|---|
| 4. Title and Subtitle<br>FINITE ELEMENT ANALYSIS AND COMPUTER GRAPHICS VISUALIZATION OF FLOW AROUND PITCHING AND PLUNGING AIRFOILS | | 5. Report Date<br>September 1973 |
| | | 6. Performing Organization Code |
| 7. Author(s)<br>Theodore Bratanow and Akin Ecer | | 8. Performing Organization Report No. |
| | | 10. Work Unit No. |
| 9. Performing Organization Name and Address<br>University of Wisconsin-Milwaukee<br>Milwaukee, Wisconsin | | 11. Contract or Grant No.<br>NGR-50-007-001 |
| | | 13. Type of Report and Period Covered<br>Contractor Report |
| 12. Sponsoring Agency Name and Address<br>National Aeronautics and Space Administration<br>Washington, D.C. 20546 | | 14. Sponsoring Agency Code |

15. Supplementary Notes

This is a Topical Report.

16. Abstract

A general computational method for analyzing unsteady flow around pitching and plunging airfoils was developed. The finite element method was applied in developing an efficient numerical procedure for the solution of equations describing the flow around airfoils. The numerical results were employed in conjunction with computer graphics techniques to produce visualization of the flow. The investigation involved mathematical model studies of flow in two phases: (1) analysis of a potential flow formulation and (2) analysis of an incompressible, unsteady, viscous flow from Navier-Stokes equations.

| 17. Key Words (Suggested by Author(s))<br>Airfoil theory<br>Computer graphics<br>Finite element method<br>Unsteady flow | 18. Distribution Statement<br><br>Unclassified - Unlimited | | |
|---|---|---|---|
| 19. Security Classif. (of this report)<br>Unclassified | 20. Security Classif. (of this page)<br>Unclassified | 21. No. of Pages<br>71 | 22. Price*<br>$3.00 |

## CONTENTS

**Page intentionally left blank**

ILLUSTRATIONS

# FINITE ELEMENT ANALYSIS AND COMPUTER GRAPHICS VISUALIZATION
## OF FLOW AROUND PITCHING AND PLUNGING AIRFOILS

By Theodore Bratanow* and Akin Ecer**
University of Wisconsin-Milwaukee

## SUMMARY

A general computational method for analyzing unsteady flow around
pitching and plunging airfoils was developed.  The finite element method
was applied in developing an efficient numerical procedure for the solu-
tion of equations describing the flow around airfoils.  Numerical results
were employed in conjunction with computer graphics techniques to produce
visualization of the flow.  The investigation involved mathematical model
studies of flow in two phases:  analysis of a potential flow formulation
and analysis of an incompressible, unsteady, viscous flow from Navier-
Stokes equations.

For the analysis of the potential flow formulation of the problem,
a finite element representation of Laplace's equation was applied.  The
potential flow model was extensively employed in reproducing patterns of
unsteady flow characteristics, in the form of computer-drawn illustrations
and computer-drawn movies.  Using the finite element method again, mathe-
matical models were further developed to analyze unsteady viscous flow
around pitching and plunging airfoils from solutions of the vorticity trans-
port equation.  A system of first order nonlinear matrix differential equa-
tions, resulting from the finite element formulation, was integrated with
respect to time to obtain vorticity distribution around airfoils.  A system
of Lagrange multipliers was applied in representing boundary conditions
around airfoils, which change with respect to time and space.  Since time-
dependent boundary conditions on airfoils were treated separately in the
formulation, the applied method produced efficient solutions of the vorti-
city transport equation, thus significantly reducing the computational
effort.

The results include computer-drawn movies and graphical representa-
tions of streaklines, streamlines, and vorticity distributions around
pitching and plunging airfoils.  Various features of the investigation,
including a detailed description of both mathematical models as well
as applied computational and computer graphics techniques, are presented.
Accuracy and advantages of the developed procedure are evaluated.

---

* Professor, ** Assistant Professor, Department of Mechanics,
College of Engineering and Applied Science.

# INTRODUCTION

The general motion of a flexible wing may consist of pitching and plunging components. The flow around the wing can be of an unsteady and three-dimensional character. A complete and clear description of such three-dimensional flows involves analytic methods applied in unsteady aerodynamics. Solutions of three-dimensional mathematical representations of such problems, as well as usable experimental data to support analytic work, are not easily obtained. Up-to-date analytic efforts have not been successful in producing desirable results. Difficulties have also been encountered in experimental work with scaling and measuring the required data. The analysis of unsteady aerodynamics problems involves solutions of nonlinear three-dimensional partial differential equations. Closed form solutions of such equations are difficult and exist only for a limited number of cases. Even with existing advanced computational facilities, numerical solutions of such problems require excessive computer time.

The purpose of the investigation was to develop mathematical models for analysis and visualization of general unsteady flow problems around pitching and plunging airfoils. The numerical results, defining the motion of the airfoil and the flow, were used in conjunction with computer graphics techniques to produce adequate visualization in time and space of the flow around the oscillating airfoil.

The overall mathematical procedure involves two major steps, which are closely related:

    I.   Mathematical model analysis

    II.  Generation of computer-drawn illustrations of flow patterns and computer-drawn movies for visualization of the flow around airfoils.

The computational procedure for the potential and unsteady viscous flow analyses can be summarized as follows:

- defining the airfoil motion and flow parameters at each time step as input

- obtaining the velocity distribution around the airfoil at each time step from the mathematical models

- numerical integration of the obtained velocity distribution to describe desired characteristics of the flow

- illustration of the flow characteristics using computer graphics techniques.

The analytical formulations were established in such a way that they were suitable for expansion in desired directions. Two-dimensional solutions of potential flow formulations proved to be most fruitful as a basis

for gaining experience and then gradually increasing the complexity of the mathematical model. The next step of the investigation was the analysis of incompressible, unsteady and viscous flow from Navier-Stokes equations. The analytically obtained flow patterns were then compared with patterns obtained by others and with actual physical flow. Nonlinearities were treated both analytically and computationally. A direct method was applied for efficient numerical solution of the equations representing the flow around the airfoil from the standpoint of computer time consumption. The finite element method was applied in a broad sense, beyond the limitations of the classical variational approach to solve the Navier-Stokes equations. The overall results were satisfactory.

The presented results are from the analysis of two-dimensional flow around a pitching and plunging airfoil. The analytical tools are in a form capable of treating general flow problems.

## SYMBOLS

| | |
|---|---|
| $A$ | area of defined region, $\text{in.}^2$ ( $\text{m}^2$ ) |
| $A_i$ | area of a triangular element, $\text{in.}^2$ ( $\text{m}^2$ ) |
| $\underline{A}$ | symmetric matrix |
| $\underline{A}_i$ | symmetric matrix for one triangular element |
| $\underline{A}^*$ | symmetric matrix containing matrix $\underline{A}$ and the boundary conditions |
| $b$ | width of a typical triangular element in figure 4, in. ( m ) |
| $\underline{b}$ | rectangular matrix representing the boundary conditions on the airfoil |
| $\underline{B}$ | row vector for the entire grid |
| $\underline{B}_i$ | row vector for a triangular element |
| $\underline{c}$ | rectangular matrix specifying the position of the nodes on the free stream boundary |
| $\underline{d}$ | column vector specifying the stream functions for the free stream boundary |

3

| | |
|---|---|
| g | $g(x,y)$ - a function specifying the boundary conditions |
| $\underline{g}$ | rectangular matrix containing matrix $\underline{b}$, $\underline{g} = (\underline{b}\ \underline{0})$ |
| h | height of a typical triangular element in figure 4, in. ( m ) |
| $\underline{h}$ | column vector containing vector $\underline{d}$, $\underline{h} = (\underline{0}\ \underline{d})$ |
| $\underline{I}$ | identity matrix |
| $\underline{0}$ | null matrix |
| p | local static pressure, psi ( $N/m^2$ ) |
| $\underline{p}$ | column vector, $\underline{p} = \underline{A}^{*-1}\ \underline{h}$ |
| $\underline{q}$ | rectangular matrix, $\underline{q} = \underline{A}^{*-1}\ \underline{g}$ |
| Q | $Q(x,y)$, $Q = -\rho\left(\dfrac{\partial^2 u^2}{\partial x^2} + \dfrac{\partial^2 uv}{\partial x \partial y} + \dfrac{\partial^2 v^2}{\partial y^2}\right)$ |
| $\underline{Q}$ | column vector representing a discrete finite element formulation of Q |
| $\underline{s}$ | a column vector |
| $\underline{S}$ | a column vector |
| t | time, sec. |
| x,y,z | coordinates, in. ( m ) |
| $x_{ij}$, $y_{ij}$ | coordinate differences, in. ( m ) |
| X,Y | body forces in x and y directions respectively, lbf ( N ) |
| u,v | velocity components of the fluid in the x and y directions respectively, in./sec. ( m/sec. ) |
| $\underline{u}$ | velocity vector, in./sec. ( m/sec. ) |
| $\nabla$ | del operator, $\nabla = \dfrac{\partial}{\partial x} + \dfrac{\partial}{\partial y}$ |

$\nabla^2$        Laplace operator, $\nabla^2 = \dfrac{\partial^2}{\partial x^2} + \dfrac{\partial^2}{\partial y^2}$

$\delta$        an eigenvalue of the triangular finite element grid

$\underline{\delta}$        column matrix representing the Lagrangian multipliers

$\gamma$        largest eigenvalue of a triangular element

$\gamma_i$        eigenvalue of a triangular element

$\nu$        kinematic viscosity coefficient, in.$^2$/sec. (m$^2$/sec.)

$\rho$        density of air, lbm/in.$^3$ (Kg/m$^3$)

$\Phi$        $\Phi(\psi)$ - quadratic function

$\psi$        $\psi(x,y)$ - stream function, in.$^2$/sec. (m$^2$/sec.)

$\underline{\psi}$        column vector representing stream function values at grid intersection points, in.$^2$/sec. (M$^2$/sec.)

$\underline{\psi}^*$        column vector, $\underline{\psi}^* = (\underline{\psi} \; \underline{\delta}_c)$

$\psi_s$        values of the stream function at a boundary, in.$^2$/sec. (m$^2$/sec.)

$\underline{\psi}_i$        column vector representing stream function values at the corners of a triangular element, in.$^2$/sec. (m$^2$/sec.)

$\omega$        $\omega(x,y)$ - vorticity function (sec.$^{-1}$)

$\underline{\omega}$        column vector representing vorticity values at the nodal points (sec.$^{-1}$)

$\underline{\omega}_i$        column vector representing vorticity values at the corners of a triangular element (sec.$^{-1}$)

Subscripts

| | |
|---|---|
| b | at the airfoil boundary |
| c | at the free stream boundary |
| h | horizontal |
| i | $i$-th triangle |
| j | $j$-th triangle |
| max | maximum |
| o | at time $t_o$ |
| p | $p$-th node |
| q | $q$-th node |
| s | at the airfoil and free stream boundaries |
| t | at time $t$ |
| v | vertical |
| x,y | derivative with respect to $x$ or $y$ |

Superscripts

| | |
|---|---|
| n | at the n-th time step |
| t | transpose |

# COMPUTER ANALYSIS AND VISUALIZATION OF FLOW PROBLEMS

## Background

A complete three-dimensional analysis of the flow around a pitching and plunging wing in flight would demonstrate the complexity of problems involving unsteady aerodynamics. Applications of numerical methods in solving unsteady aerodynamics flow problems have received considerable attention during recent years [refs. 1, 2, 3, 4, 5, 6]. Attempts have also been reported of solving three-dimensional flow problems numerically by considering them as two-dimensional ones and then including only linear effects of the third dimension [refs. 7, 8, 9]. Some approximate solutions have been obtained from linearized forms of three-dimensional flow formulations. In each instance, however, a clear understanding of the kinematics of the three-dimensional flow was required in order to obtain realistic results. Some investigations have involved application of finite difference techniques and have yielded encouraging but limited results. Applications of finite difference techniques did not become very popular because of the amount of computer time required for satisfactory results. Also, in some reported investigations theoretical and experimental methods have been used conjunctionally.

The finite element method was originally applied in the field of solid mechanics. Availability of variational formulations for some of the basic solid mechanics problems encouraged researchers to take advantage of such formulations in applying the finite element method. It should be pointed out, however, that variational formulations may not be the only basis for finite element applications. The application is essentially a representation of a continuum by discrete finite elements and setting up governing equations of the dynamics problem in terms of discrete displacements, velocities and accelerations at elemental nodal points.

The finite element method has already been applied for solution of flow problems [refs. 10, 11, 12, 13, 14]. Early applications favored problems for which variational formulations existed. Examples are: seepage flow, heat conduction and potential flow problems which involve solutions of Laplace's equation. Many reported attempts at solving general flow problems encountered difficulties with the nonlinearities involved in the Navier-Stokes equations. Some flow problem formulations [refs. 15, 13] have been based on the concept of "local potential", as introduced by Glansdorff and Prigogine [ref. 16]. In such applications the energy and momentum can be minimized in a finite region, for which equations of motion can be obtained.

Oden [ref. 12] has applied the finite element method for general problems involving slow viscous flow. The variational formulation was based on minimum viscous dissipation as described by the Helmholtz equation. The

solutions are of the type obtained from Dirichlet's problem. The formulation is concise, and accuracy of the results is satisfactory. Bowley and Prince [ref. 10] developed a numerical procedure which uses a finite element technique. They applied the integral form of the time dependent equations of mass, (x- and y-) momenta, and energy conservation to various subdomains of the whole region. The results were also satisfactory.

In 1963 Fromm [ref. 3] applied the Helmholtz vorticity transport equation in conjunction with the finite difference method to analyze unsteady incompressible flow at various Reynolds numbers around stationary objects. Derivatives in the Helmholtz equation were replaced with central differences both in space and time. A successive approximation technique was applied to obtain the streamfunction, which satisfies Poisson's equation. Fromm's results demonstrated in a spectacular way the feasibility of such a technique; however, the applied numerical solution contained already known deficiencies of the finite difference method. The applied iterative scheme slows down the computational process. Even more significant is the difficulty connected with the representation of a moving obstacle having a curved boundary, as is the case with an oscillating airfoil. Obtaining a reasonably accurate solution of such problems by applying finite difference methods seems to be uneconomical.

Various experimental techniques have been applied in attempts to visualize and measure unsteady flow around airfoils in the laboratory; only limited results were obtained and correlation was poor. It is not known if other efforts have been made for the flow visualization problem of a pitching and plunging airfoil in conjunction with a theoretical analysis, involving a finite element method and computer graphics techniques.

Mathematical Analysis

The procedure followed in the mathematical model analysis involves mainly:

.   solutions of a potential flow representation of the flow patterns around oscillating airfoils

.   solutions of Navier-Stokes equations for representation of patterns of unsteady, incompressible, viscous flow around pitching and plunging airfoils.

Potential flow analysis. - Numerical techniques were applied to obtain solutions of the potential flow representation. The procedure for the potential flow analysis will now be summarized. Streamfunctions in the flow field were defined as

$$u = \frac{\partial \psi}{\partial y} \qquad v = -\frac{\partial \psi}{\partial x} \qquad (1)$$

where the streamfunctions satisfy Laplace's equation

$$\nabla^2 \psi = 0 \qquad (2)$$

for prescribed conditions

$$\psi_s = g \qquad (3)$$

on airfoil boundaries and on imaginary boundary lines representing the undisturbed flow.

The developed numerical procedure for solution of the system of equations (1), (2), and (3) was based on the finite element method [ref. 17]. Details of the mathematical model and the numerical analysis are summarized in Appendix A.

Unsteady, viscous flow analysis. - Solutions for unsteady, incompressible and viscous flow are obtained from Navier-Stokes equations as a refinement of the potential flow model. The system of vorticity transport equation and Poisson's equation applied in the analysis of flow around an oscillating airfoil is

$$\frac{\partial \omega}{\partial t} + \frac{\partial}{\partial x}\left(u\omega - \nu \frac{\partial \omega}{\partial x}\right) + \frac{\partial}{\partial y}\left(v\omega - \nu \frac{\partial \omega}{\partial y}\right) = 0 \qquad (4)$$

$$\nabla^2 \psi = -\omega \qquad (5)$$

Equations (4) and (5) were solved simultaneously for the same time step, whereby equation (4) was integrated with respect to time, to obtain vorticity distribution around oscillating airfoils. The finite element method was applied again in obtaining a numerical solution. The developed numerical method is quite general and can be applied in analyzing flow around obstacles of any shape under arbitrary motion. Detailed description of the mathematical model as well as the applied numerical method is presented in Appendix B.

Details of the Mathematical Analysis

Figures 1a and 1b illustrate the important features of the applied analysis of mathematical models for potential flow and unsteady viscous

flow. The two- and three-dimensional potential flow formulations and analyses are very useful first approximations of flow patterns around oscillating airfoils [ref. 11]. However, the representations of the flow are general and do not account for the effects of the boundary layers.

The finite element method was applied for both the numerical solution of the potential flow formulation, equations (1), (2), (3), and the numerical solution of the unsteady viscous flow formulation, equations (4) and (5). The numerical procedure for the treatment of Poisson's equation, equation (5), for both potential and unsteady viscous flow is direct and requires no iteration. The input data for the mathematical models describe the geometry of the obstacle and the free stream characteristics of the flow in a most general form. The exact shape of an airfoil and its motion are represented in their actual form, without any approximation.

Initially, the vorticity distribution for each of the cases was unknown. Therefore, at the beginning of each numerical integration process, the vorticity distribution was assumed to be unity at a point approximately one half chord length upstream of the airfoil and zero for the remaining region around the airfoil. With the initially assumed vorticity distribution, Poisson's equation was solved for stream functions and then the vorticity transport equation was integrated with respect to time. The numerical integration was advanced with respect to time and the flow characteristics at each time step were recorded. This process was continued until the numerical integration reached a steady state; i.e., when the changes in the vorticity distribution with respect to time were no longer significant. The steady state condition was then used as an initial condition for analyzing the unsteady flow around oscillating airfoils.

The vorticity distribution around the airfoil was obtained from the numerical integration with respect to time of a system of first order nonlinear matrix differential equations. The time-dependent boundary conditions in the solution of the vorticity transport equation and Poisson's equation were treated in a way to minimize computational cost. The boundary conditions around the obstacle in the flow field, which vary in time and space coordinates, were represented by resorting to the Lagrange multiplier technique. Doing so allowed for a separation of the boundary conditions in both the solution of the vorticity transport equation and Poisson's equation. Terms which are independent of time were kept in computer storage throughout the entire numerical integration process in order to avoid excessive computer time consumption.

For the solution of the potential flow, the region on and around the obstacle in the flow field was defined by a finite element triangular grid as shown in figures 2a, 2b, and 2c. For each of the triangular elements in this grid, the variational form of Laplace's equation was developed. Around the leading edge of the airfoil, where the variation of the stream functions is most intense, a finer mesh was adopted. As the airfoil undergoes pitching and plunging motion, the entire grid can be rotated by simply changing the boundary conditions on the outside rectangle representing the free stream flow.

10

Another mesh, shown in figure 3, was used for the unsteady viscous flow analysis obtained from the Navier-Stokes equations. As can be seen from the figure, the arrangement of this mesh is not dependent on the positions of the airfoil. The boundary conditions on the airfoil are related to this mesh by simply setting prescribed values of stream functions and vorticities at certain points of the grid, using Lagrange multipliers. In the analysis of the flow around a circle, for example, the geometry of the circular obstacle is superimposed on the mesh. The motion of the obstacle can be described by redefining the boundary conditions on the obstacle for equations (4) and (5), at each time step of the numerical integration of equation (4). These boundary conditions are then applied on the system of matrix differential equations, as obtained from the finite element representation of the governing differential equation. Solutions of the discretized form of Poisson's equation and the vorticity transport equation, at each time step, are then reduced to the solution of a system of linear algebraic equations.

Using a Lagrange multiplier technique the system of linear algebraic equations can be written in matrix form as

$$
\begin{bmatrix} \underline{A} & \underline{b}^t \\ \\ \underline{b} & \underline{0} \end{bmatrix} \begin{bmatrix} \underline{s} \\ \\ \underline{\delta} \end{bmatrix} = \begin{bmatrix} \underline{S} \\ \\ \underline{0} \end{bmatrix} \tag{6}
$$

As the numerical integration proceeds, matrices $\underline{S}$ and $\underline{b}$ change with respect to time, depending on the instantaneous position of the obstacle. However, matrix $\underline{A}$ does not change with respect to time and can be inverted right at the beginning of the analysis and stored in the computer. The solution vector $\underline{s}$ represents the streamfunctions in the solution of Poisson's equation and the rate of change of vorticities in the solution of the vorticity transport equation.

The solution then consists of:

  .     assembling matrix $\underline{S}$, which represents the vorticity distribution for the solution of Poisson's equation and the unsteady and viscous terms of the vorticity transport equation

  .     defining matrix $\underline{b}$ for a given shape of the obstacle and its instantaneous position

  .     performing numerical integration of the discretized form of the vorticity transport equation.

In the case of steady flow, the problem is simplified, since matrix $\underline{b}$ does not change with respect to time. Considering that the order of matrix $\underline{A}$ turns out to be much larger than that of matrix $\underline{b}$, the presented technique yields satisfactory results.

## The Computer-Generated Movies

Computer-generated movies offer definite advantages in visualization of solutions of time-dependent engineering problems. An exact interpretation of time-dependent results is faciliated by such visualization as these movies provide. Streamlines, streaklines, and pathlines were used in the flow visualization studies. Although such kinematic concepts are effective in flow visualization, a more forceful representation of flow patterns is a movie showing the actual flow as it occurs; details of the motion can thus be depicted which are not easy to observe directly.

Computer-generated movies are a direct product of analysis of mathematical models, for which assumptions and problem conditions are well defined. The accuracy of results obtained using computer graphics visualization techniques depends only on the accuracy of the developed mathematical model. The various parameters defining the motion of the fluid can be visualized in time and space. The observation can take place in any reduced time system, and details of the flow can be magnified and projected in any desired coordinate system. Simply by adjusting input parameters in the computer program, one can obtain a desirable view of the process and observe the effects of the individual physical parameters of the mathematical model. Corrections and improvements in the mathematical model can be observed immediately from the computer-drawn movies.

Once the analysis of the mathematical model for the motion of the oscillating airfoil and the flow renders acceptable results, these results are used as input to produce computer-drawn movies. The computer graphics procedures developed for the flow visualization analysis were summarized in two main steps, as shown in figure 1c. The triangular grids shown in figures 2a, 2b, and 2c, which were used for the finite element analysis of potential flow, were used again for determining the motion of the fluid particles. The computer program first records the position of a fluid particle, which starts from a reference position, by determining in which triangular element the particle is located. The magnitude and direction of the velocity at that point is obtained from the output of the mathematical model; the motion of the particle is defined through numerical integration of this velocity vector with respect to time. Then, using analytic and computer graphics techniques the positions of a large number of fluid particles and the position of the obstacle at a particular respective time instant are projected on a frame.

Results can be compared and correlated with actual flow information obtained from experimental studies and the mathematical model can again be improved. Such improvements are not easily made in an experimental procedure. Thus, a direct link can be established between experimental and theoretical studies.

To achieve a satisfactory yet economical representation of the problem, it was necessary to scrutinize each individual sequence of the two analyses and their interrelation. A 4020 Stromberg-Carlson data graphics device was

used to generate the computer-drawn movies.  The major portion of the computational work was carried out at the University of Wisconsin-Milwaukee on a UNIVAC 1108 computer.

## Discussion of the Results

The results presented in this report were obtained from two-dimensional formulations of flow around airfoils in conjunction with computer graphics techniques.  Physical and numerical aspects of unsteady flow problems were investigated.  The presented data were chosen to show the suitability of the developed method for visualization of flow around pitching and plunging airfoils.  The actual form of the airfoil was accurately represented.  The airfoil used in the analysis for flow visualization was NACA 0012 airfoil.  Several cases involving application of Poisson's equation and Navier-Stokes equations were analyzed.  The results include streamlines, streaklines, vorticity distributions, and computer-generated movies.

The movies depict accurately the effects of the pitching and plunging motion of the airfoil on the overall flow patterns around the airfoil.  The production cost for the sample movies was quite moderate.  The longest movie consisted of six sections, each 15 seconds long, and depicted the following cases:

1) pitching of the airfoil through angles of attack $\pm 8°$

2) plunging of the airfoil through $\pm 85\%$ of the airfoil chord thickness

3) pitching of $\pm 8°$ and plunging of $\pm 85\%$ chord thickness (the basic case)

3a) same as in case 3 except that the plunging is $\pm 42\%$ of chord thickness

3b) same as in case 3  except that the free stream velocity is reduced by 50%

3c) same as in case 3 except that the pitching and plunging motion is 180° out of phase.

An illustration of a few sample frames from a movie are shown in figure 4.

The vorticity distribution around a NACA 0012 airfoil was obtained from the solution of the vorticity transport equation and Poisson's equation, as a direct output of the computer program.  The different physical conditions for the numerical integration of the equations were:

. Reynolds numbers $10^2$, $10^3$, $10^5$

. pitching amplitude  0° (static), 0°±4°, 0°±8°

. plunging amplitude  ±42% and ±85% of chord thickness

13

.    different initial location of the starting vortex

.    timewise variation of the flow parameters.

Computer graphics techniques were used to produce visualization of
the vorticity distribution around the airfoil at successive time steps.
The numerical results for the vorticity distribution around the airfoil,
at various time steps, were plotted using a contour routine, as shown in
figures 5-11.  As can be seen from these figures, the initially imposed
vortex diffuses around the airfoil with advancing time.  The boundary
conditions around a moving airfoil were described quite accurately during
the calculations as can be seen for example from figure 11.  The moving
vortex in this figure follows quite closely the motion of the airfoil.

The sample cases in figures 5-11 indicate:

.    difference in the overall behavior of the flow at different
     Reynolds numbers and angles of attack

.    influence on flow patterns due to pitching and plunging os-
     cillations of the airfoil

.    behavior of a vortex after it strikes an airfoil

.    growth and decay of unsteadiness of the flow in areas where
     vorticity distribution increases.

Figures 12 and 13 show computer-drawn illustrations of streamlines and
streaklines.  The streamlines were obtained from calculated values of the
stream functions at particular time intervals by simply drawing contour
lines.  In figure 12 unsteady flow streamlines obtained from solutions of
Navier-Stokes equations are shown at various angles of attack of the airfoil.
Streaklines, as shown in figure 13, were obtained by plotting instantaneous
positions of a numer of flow particles, which have passed through a fixed
point in the free stream.  After the velocity distribution around the air-
foil at each time step was determined these values were integrated to obtain
the position of each fluid particle.  Comparisons of computer time required
for the application developed here and finite difference applications have
demonstrated the advantage of the developed procedure (See table 1).

Concluding Remarks

The developed computational method has dealt effectively with dif-
ficulties involved in solutions of equations representing unsteady flow
patterns around pitching and plunging airfoils.  The combined application
of finite element method and the chosen numerical procedure, for both the
analytic and graphics calculations, have provided a strong and flexible
tool for producing desirable results at a reasonable computational cost.

14

The important advantages of the developed computational method can be summarized as follows:

- solution of Poisson's equation by a direct method, without any iteration, for both potential and unsteady viscous flow analyses

- separate treatment of time-dependent boundary conditions related to oscillating airfoils, for both solution of Poisson's equation and numerical integration of the vorticity transport equation

- capability to relate mathematical flow analysis directly to flow visualization

- capability to represent boundary conditions on an obstacle of arbitrary shape.

Experimental results applicable to flow visualization studies in unsteady aerodynamics are limited. The developed procedure for flow visualization has the potential of linking more effectively theoretical and experimental studies by filling the wide gap, which exists in many instances between results of the two investigative methods. The unsteady flow problem around an oscillating rotor blade airfoil is a most instructive example for such applications. A complete package of analysis and visualization of the flow around a pitching and plunging airfoil offers a new tool in aerodynamic studies.

APPENDIX A

FINITE ELEMENT ANALYSIS OF POTENTIAL FLOW
AROUND AN OSCILLATING AIRFOIL

Method of Solution

The solution of the problem represented by equations (2) and (3) can
be reduced to finding the minimum of the integral

$$\Phi(\psi) = \int_A \left[ \left(\frac{\partial \psi}{\partial x}\right)^2 + \left(\frac{\partial \psi}{\partial y}\right)^2 \right] \, dA \tag{A1}$$

where $\psi$ is a function of x and y which satisfies the boundary conditions
in equation (3) [refs. 18, 19, 20].

The finite element method was applied for evaluation of the integral
in equation (A1). The volume of air around the airfoil and the airfoil,
accordingly, were represented by a series of triangles as shown in figure
2.

The curved geometry of the airfoil boundary was considered in assem-
bling the finite element grid. Once the finite element grid was devel-
oped, it was assumed that the values of the streamfunctions vary line-
arly over the area of each of the finite element triangles. Although a
finite element model of a higher order could be used, in this case even a
lower order model has provided quite accurate results.

When a linear variation of the streamfunctions is assumed for a tri-
angle as shown in figure 14, the streamfunction at any point (x, y) can
be written as

$$\psi(x,y) = [B_1 \; B_2 \; B_3] \begin{bmatrix} \psi_1 \\ \psi_2 \\ \psi_3 \end{bmatrix} = \underline{B}_i \underline{\psi}_i \tag{A2}$$

In equation (A2) the elements of row rector $\underline{B}_i$ are first order poly-
nomials in terms of x and y. The derivative of the streamfunction $\psi$ in
x and y directions can be calculated as follows:

$$\frac{\partial \psi}{\partial x} = [B_{1x} \quad B_{2x} \quad B_{3x}] \begin{bmatrix} \psi_1 \\ \psi_2 \\ \psi_3 \end{bmatrix} = \underline{B}_{ix} \underline{\psi}_i \qquad (A3)$$

and

$$\frac{\partial \psi}{\partial y} = [B_{1y} \quad B_{2y} \quad B_{3y}] \begin{bmatrix} \psi_1 \\ \psi_2 \\ \psi_3 \end{bmatrix} = \underline{B}_{iy} \underline{\psi}_i \qquad (A4)$$

The integral in equation (A1) can now be evaluated in a series form as

$$\Phi(\psi) = \sum_{i=1}^{n} \underline{\psi}_i^t \left( \underline{B}_{ix}^t \underline{B}_{ix} + \underline{B}_{iy}^t \underline{B}_{iy} \right) \underline{\psi}_i A_i \qquad (A5)$$

where the subscript i indicates summation of respective terms for each of the finite element triangles.

After applying the principle of minimum potential energy, the solution of Laplace's equation for the defined finite element grid can be obtained from the following system of linear algebraic equations:

$$[\underline{0}] = \sum_{i=1}^{n} A_i \left( \underline{B}_{ix}^t \underline{B}_{ix} + \underline{B}_{iy}^t \underline{B}_{iy} \right) \underline{\psi}_i = \underline{A} \, \underline{\psi} \qquad (A6)$$

The matrix $\underline{A}$ resulting from equation (A6) is a singular matrix. The boundary conditions around the airfoil and at the free stream boundaries have to be applied to obtain a unique solution to the problem. Once the stream functions at the nodes of the triangles are calculated, a set of streamlines passing above and under the oscillating airfoil can be drawn as the contour lines for the calculated values of stream functions (figure 12).

## Boundary Conditions

The boundary conditions shown in equation (3) can be described in two steps.

Boundary conditions on the airfoil. - According to the potential flow theory, the velocity vectors on the airfoil boundary are tangent to the airfoil surface. In other words, the boundary of the airfoil forms a streamline. This boundary condition can be imposed on the discretized system by introducing the following relation:

$$\psi_p - \psi_q = 0 \tag{A7}$$

The constraining relation (A7) simply implies that stream functions at neighboring nodes are equal.

Boundary conditions for free stream boundary. - The second type of boundary conditions are those defining free stream conditions around the considered flow field (outer boundaries). The flow around the airfoil can be represented for various angles of attack by specifying the stream functions at the nodes of the rectangular outer boundary, in desired positions. In a computational sense, this can be considered equivalent to rotating the entire rectangular frame in figure 2, instead of oscillating the airfoil. Thus, it is possible to use the same matrix $\underline{A}$ in equation (A6) throughout the analysis and save considerable computer time.

Solution of the System of Equations

The boundary conditions corresponding to the system of equations shown in equation (A6) can be added, as an additional constraint, in matrix form as follows:

$$\underline{b}^t \, \underline{\psi} = \underline{0} \tag{A8}$$

on the airfoil and

$$\underline{c}^t \, \underline{\psi} = \underline{d} \tag{A9}$$

on the free stream boundaries. The total system of equations for the potential flow analysis can now be written as follows:

$$\begin{bmatrix} \underline{A} & \underline{c} & \underline{b} \\ \underline{c}^t & \underline{0} & \underline{0} \\ \underline{b}^t & \underline{0} & \underline{0} \end{bmatrix} \begin{bmatrix} \underline{\psi} \\ \underline{\delta}_c \\ \underline{\delta}_b \end{bmatrix} = \begin{bmatrix} \underline{0} \\ \underline{d} \\ \underline{0} \end{bmatrix} \tag{A10}$$

In potential flow analysis, the $\underline{A}$, $\underline{c}$ and $\underline{d}$ matrices are constant while the matrix $\underline{b}$ changes with the position of the airfoil. If the $\underline{A}$ and $\underline{c}$ matrices are combined, equation (A10) can be expressed as follows:

$$\begin{bmatrix} \underline{A}^* & \underline{g} \\ \underline{g}^t & \underline{0} \end{bmatrix} \begin{bmatrix} \underline{\psi}^* \\ \underline{\delta}_b \end{bmatrix} = \begin{bmatrix} \underline{h} \\ \underline{0} \end{bmatrix} \tag{A11}$$

where

$$\underline{A}^* = \begin{bmatrix} \underline{A} & \underline{c} \\ \underline{c}^t & \underline{0} \end{bmatrix} \qquad \underline{g} = \begin{bmatrix} \underline{b} \\ \underline{0} \end{bmatrix} \qquad \underline{h} = \begin{bmatrix} \underline{0} \\ \underline{d} \end{bmatrix} \tag{A12}$$

Here $\underline{\delta}_b$ is a column matrix consisting of Lagrangian multipliers corresponding to the boundary conditions on the airfoil surface. In this case matrix $\underline{A}^*$ corresponds to the free stream flow, is not singular, and can be inverted to obtain the stream functions for the free stream flow.

$$\underline{\psi}^* = \underline{p} - \underline{q} \ [\underline{g}^t \ \underline{q}]^{-1} \ \underline{g}^t \underline{p} \tag{A13}$$

where

$$\underline{p} = \underline{A}^{*-1} \ \underline{h} \tag{A14}$$

$$\text{and} \qquad \underline{q} = \underline{A}^{*-1} \ \underline{g} \tag{A15}$$

Since matrices $\underline{A}^*$ and $\underline{h}$ are constant for the potential flow, at each time interval only the matrices $\underline{g}$ and $\underline{q}$ have to be calculated. In cases where the entire triangular grid was rotated to represent the motion of the airfoil, the matrix $\underline{b}$ becomes a constant matrix, while the $\underline{c}$ and $\underline{d}$ matrices are calculated at each time interval.

The effects of different types of obstacles in the flow field can be determined from the solution routine by defining a different $\underline{b}$ matrix and using the same $\underline{A}^{*-1}$ matrix. Here again the $\underline{b}$ matrix represents the geometry of the obstacle and the $\underline{A}^{*-1}$ matrix represents the free stream flow.

19

# APPENDIX B

## FINITE ELEMENT ANALYSIS OF UNSTEADY
## FLOW AROUND AN OSCILLATING AIRFOIL

### Mathematical Description of the Problem

Governing differential equations. - To analyze unsteady flow around an oscillating airfoil, one has to solve the Navier-Stokes equations for incompressible viscous fluid, which can be written as follows:

$$\frac{\partial u}{\partial t} + u\frac{\partial u}{\partial x} + v\frac{\partial u}{\partial y} = \frac{1}{\rho}X - \frac{1}{\rho}\frac{\partial p}{\partial x} + \nu\left\{\frac{\partial^2 u}{\partial x^2} + \frac{\partial^2 u}{\partial y^2}\right\} \qquad (B1)$$

$$\frac{\partial v}{\partial t} + u\frac{\partial v}{\partial x} + v\frac{\partial v}{\partial y} = \frac{1}{\rho}Y - \frac{1}{\rho}\frac{\partial p}{\partial y} + \nu\left\{\frac{\partial^2 v}{\partial x^2} + \frac{\partial^2 v}{\partial y^2}\right\} \qquad (B2)$$

The required additional condition of continuity can be written as

$$\frac{\partial u}{\partial x} + \frac{\partial v}{\partial y} = 0 \qquad (B3)$$

The boundary conditions on the airfoil can be defined as $u = v = 0$. The velocity distribution on the outer rectangular boundary can be prescribed from the free stream conditions.

Equations (B1) and (B2) can now be expressed in a convenient form by introducing an additional variable to define vorticity as

$$\omega = \frac{\partial v}{\partial x} - \frac{\partial u}{\partial y} \qquad (B4)$$

Equations (B1) and (B2) can be combined as the Helmholtz equation

$$\frac{\partial \omega}{\partial t} + \frac{\partial}{\partial x}\left(u\omega - \nu\frac{\partial \omega}{\partial x}\right) + \frac{\partial}{\partial y}\left(v\omega - \nu\frac{\partial \omega}{\partial y}\right) = 0 \qquad (B5)$$

Equation (B5) is also known as the "vorticity transport" equation.

To satisfy the equation of continuity another variable will be introduced by defining the stream function as

$$u = \frac{\partial \psi}{\partial y} \qquad\qquad v = - \frac{\partial \psi}{\partial x} \qquad\qquad (B6)$$

The equation of continuity is then automatically satisfied. From equation (B4) the vorticity can be related to the stream function as follows:

$$\omega = - \nabla^2 \psi \qquad\qquad (B7)$$

The values of the stream functions are known for the free stream boundary and are made equal to each other on the airfoil boundary.

From the above formulation the finite element method can be applied for the solution of incompressible flow problems. Examples of such applications are these:

a) potential flow; can be analyzed with equation (B7) for vanishing vorticity terms (Appendix A)

b) steady state flow; can be analyzed from equations (B5) and (B7) by numerical integration of equation (B5) until a stable solution is obtained

c) unsteady flow; requires the simultaneous solution of equations (B5) and (B7) and numerical integration of equation (B5).

Once the velocity distribution has been determined, the corresponding pressure distribution may also be calculated from the following expression:

$$\frac{\partial^2 p}{\partial x^2} + \frac{\partial^2 p}{\partial y^2} = - \rho \left\{ \frac{\partial^2 u^2}{\partial x^2} + 2 \frac{\partial^2 uv}{\partial x \partial y} + \frac{\partial^2 v^2}{\partial y^2} \right\} \qquad\qquad (B8)$$

Method of solution. - The mathematical analysis of unsteady flow problems can be carried out in the following manner:

a) determine initial vorticity distribution

b) calculate stream functions from equation (B7)

c) determine velocity distribution in x- and y- directions from equation (B6)

d)  integrate equation (B5) with respect to time to obtain the vorticity distribution at time t + Δt

e)  repeat steps b, c, and d for each time increment.

The initial vorticity distribution is usually unknown. Therefore starting from an arbitrary vorticity distribution for the initial stationary airfoil position, the procedure is repeated until a steady state solution is obtained.

A numerical procedure based on the finite element method, was applied for each one of the above steps.

### Analysis of the Vorticity Transport Equation

A finite element representation of an oscillating airfoil and the surrounding air flow is shown in figure 3 by a triangular mesh system. Velocity and vorticity distributions around the airfoil are defined at the nodes for each triangular element. The numerical method can be outlined in the following steps.

The finite element. -A basic finite element model was chosen initially to examine the method of solution. It was assumed that vorticity and stream function values vary linearly over the area of each triangular element. Then, for a typical triangular element, shown in figure 15, the vorticity and the stream function at any point on the triangle are defined by

$$\omega = \begin{bmatrix} B_1 & B_2 & B_3 \end{bmatrix} \begin{bmatrix} \omega_1 \\ \omega_2 \\ \omega_3 \end{bmatrix} = \underline{B}_i \underline{\omega}_i \tag{B9}$$

and

$$\psi = \begin{bmatrix} B_1 & B_2 & B_3 \end{bmatrix} \begin{bmatrix} \psi_1 \\ \psi_2 \\ \psi_3 \end{bmatrix} = \underline{B}_i \underline{\psi}_i \tag{B10}$$

The solution of Poisson's equation. - Knowing the vorticity distribution around the airfoil, one can determine the stream functions from the finite element solution of Poisson's equation. The solution of this equation can be obtained as described in Appendix A. The quadratic function to be minimized is obtained from the variational formulation of equation (B7) as

$$\Phi = \frac{1}{2} \int_A \left\{ \left(\frac{\partial \psi}{\partial x}\right)^2 + \left(\frac{\partial \psi}{\partial y}\right)^2 \right\} \, dA - \int_A \omega\psi \, dA \tag{B11}$$

Substitution of equations (B9) and (B10) into (B11) yields

$$\int_A \left\{ \underline{B}_x^t \, \underline{B}_x + \underline{B}_y^t \, \underline{B}_y \right\} \, dA \; \underline{\psi} = \int_A \underline{B}^t \, \underline{B} \, dA \; \underline{\omega} \tag{B12}$$

The solution of equation (B12) provides the stream functions at the nodal points, and thus the velocity distribution around the airfoil. The next step is the numerical integration of equation (B5).

Variational formulation of the vorticity transport equation. - The exact variational formulation of the vorticity transport equation does not exist due to the nonlinearities in the equation; containing both velocities and derivatives of vorticities. Although the linear terms in equation (B5) can be written in variational form quite readily, one has to treat the velocities u and v as functions of the vorticity distribution $\omega$. A perturbation technique for treating such nonlinearities has been applied by Ecer [ref. 21] to finite element analysis of buckling problems in solid mechanics and has produced satisfactory results. For the variational formulation of the vorticity transport equation, a similar technique can be applied. By using a Taylor series expansion of the velocities in terms of the vorticity distribution, at a particular time $t_o$, the velocity distribution becomes

$$\underline{u} = \underline{u}_o + \left(\frac{\partial \underline{u}}{\partial \omega}\right)_o \Delta\omega + \left(\frac{\partial^2 \underline{u}}{\partial\omega^2}\right)_o \frac{(\Delta\omega)^2}{2!} + \left(\frac{\partial^3 \underline{u}}{\partial\omega^3}\right)_o \frac{(\Delta\omega)^3}{3!} + \ldots \tag{B13}$$

The problem is thus reduced to calculating derivatives of the velocity distribution in terms of vorticities. This can be done readily from the finite element formulation of Poisson's equation. The equations of continuity and vorticity can be written as

$$\nabla \cdot \underline{u} = 0 \qquad\qquad\qquad \nabla \times \underline{u} = \underline{\omega} \tag{B14}$$

from which

$$\nabla \cdot \frac{\partial \underline{u}}{\partial \omega} = \underline{0} \qquad\qquad\qquad \nabla \times \frac{\partial \underline{u}}{\partial \omega} = \underline{I} \tag{B15}$$

Using equation (B15) calculation of the first derivative of the velocity vector can be obtained from the solution of Poisson's equation for a unit vorticity, at each of the nodes of the triangular grid. Higher order derivatives can also be defined in a similar manner, again from the solution of Poisson's equation. As described in Appendix A, this procedure does not require excessive amount of computations, since the solution of the equations for free stream conditions (A13) is already stored in the computer. Only the first term in the Taylor series was initially kept, since the velocity distribution is not very sensitive to the changes in vorticity distribution. The integral functional to be minimized in this case can be written as follows:

$$\phi = \int_A \omega \frac{\partial \omega}{\partial t} dA + \frac{1}{2} \int_A u\omega \frac{\partial \omega}{\partial x} dA + \frac{1}{2} \int_A v\omega \frac{\partial \omega}{\partial y} dA + \frac{\nu}{2} \int_A \left[ \left(\frac{\partial \omega}{\partial x}\right)^2 + \left(\frac{\partial \omega}{\partial y}\right)^2 \right] dA \quad (B16)$$

For a triangular element, with a linear variation of vorticity and stream functions, equation (B16) can be discretized in finite element form as follows:

$$\int_A \underline{B}^t \underline{B} \, dA \, \frac{\partial \underline{\omega}}{\partial t} = - \int_A \left\{ \nu \left[ \underline{B}_x^t \underline{B}_x + \underline{B}_y^t \underline{B}_y \right] + u \, \underline{B}^t \underline{B}_x + v \, \underline{B}^t \underline{B}_y \right\} dA \, \underline{\omega} \quad (B17)$$

The vorticity transport equation can then be solved by numerical integration of the system of difference equations in (B17).

Boundary conditions. - The boundary conditions to be satisfied by the finite element model are these:

$\psi$ - prescribed on the rectangular outer boundary as shown in figure 3

$\psi$ - constant on the airfoil boundary

$\omega = 0$ on the rectangular outer boundary and on the boundary of the airfoil.

A Lagrange multiplier technique was used in the solution of the unsteady flow equations to satisfy the above boundary conditions.

A different grid was prepared for the finite element analysis as shown in figure 3. Elements of smaller size were used for the inner region of the rectangular grid, where the airfoil was pitching and plunging. The shape of the airfoil was defined by specifying coordinates of a series of points where the airfoil boundary conditions are satisfied. The boundary conditions for stream functions around the airfoil can be satisfied by

24

requiring that all points on the airfoil boundary have equal values. The boundary conditions used to specify vorticities on the airfoil and on the rectangular outer boundary can be satisfied by setting the vorticity values at these points equal to zero. All these boundary conditions are included in the solution of Poisson's equation and the vorticity transport equation as supplementary constraint equations. As the position of the airfoil changes, coordinates of new points are defined to describe the airfoil; thus only the constraint equations need to be changed at different time increments.

The direction of the velocity vectors on the boundary of a moving airfoil is a function of the motion of the airfoil. This problem can thus be treated by using a higher order finite element model, having velocities as unknowns at each node. In such cases the direction of the velocity vectors can be defined at each node, considering also the motion of the airfoil. As the numerical integration interval becomes smaller, however, both solutions converge.

Numerical integration of the vorticity transport equation. - The numerical solution of the difference equation (B17) can be obtained by applying well-known numerical techniques [ref. 22]. Fromm [ref. 3] has experimented with various difference techniques and has studied the stability of these equations with respect to various parameters. Roache and Mueller [ref. 6] applied a similar method for the solution of the vorticity transport equation, as obtained from a finite difference approximation. However, none of the above attempts yielded the clear and effective representation of governing time-dependent equations as obtained from the finite element method. Time-dependent boundary conditions can be imposed on equation (B17) as an additional constraint, as explained above. The change of airfoil boundary conditions with respect to time can be introduced by specifying that the vorticities are equal to zero for the new position of the airfoil at time $t = t_o + \Delta t$. Using an Euler method of integration, the vorticity distribution at time $t + \Delta t$ can be written as

$$\omega_{t + \Delta t} = \omega_t + \frac{\partial \omega_t}{\partial t} \Delta t \tag{B18}$$

or writing equation (B18) in matrix form as

$$\underline{\omega}_{t + \Delta t} = \underline{\omega}_t + \underline{A}\,\underline{\omega}_t\,\Delta t \tag{B19}$$

When the vorticity transport equation is solved from the finite element formulation to obtain

$$\frac{\partial \underline{\omega}}{\partial t} \quad \text{at } t = t_0$$

the problem reduces to numerical integration of a nonlinear discrete system with respect to time. The nonlinear system is defined for the $n^{th}$ time step by

$$\frac{d\underline{\omega}^n}{dt} = \underline{A} \, \underline{\omega}^n \tag{B20}$$

and under the boundary conditions

$$\frac{d\underline{\omega}^n}{dt} = \frac{1}{\Delta t} \left[ \underline{\omega}^{n+1} - \underline{\omega}^n \right]_s \tag{B21}$$

Standard numerical techniques were applied for solving the above system of difference equations (B20) and (B21). Formulations based on a finite difference approximation become intractable as a higher order integration technique is used for the solution of the time-dependent problem. In the presented approach, based on a finite element formulation, time and space variables are separated. The resulting difference equations can be integrated by any of the recognized numerical integration techniques, where the elements of an error analysis are well defined.

Calculation of pressures around the airfoil. - Finally, the pressures around the airfoil can be calculated from the finite element solution of equation (B8). To increase the accuracy of the solution, a higher order finite element model can be employed. An improved finite element model requires a higher order approximation of the stream functions, while allowing vorticities to vary linearly over the triangular element. The stream functions and their derivatives at the nodes can be defined as

$$\left[ \psi_1 \quad \frac{\partial \psi_1}{\partial x} \quad \frac{\partial \psi_1}{\partial y} \quad \psi_2 \quad \frac{\partial \psi_2}{\partial x} \quad \frac{\partial \psi_2}{\partial y} \quad \psi_3 \quad \frac{\partial \psi_3}{\partial x} \quad \frac{\partial \psi_3}{\partial y} \right] \tag{B22}$$

In the above example the number of equations in matrix equation (B7) will be increased three times. However, the method of solution remains the same. The distribution of velocity is then assumed to be linear over the triangular element as follows:

$$u = \begin{bmatrix} B_1 & B_2 & B_3 \end{bmatrix} \begin{bmatrix} u_1 \\ u_2 \\ u_3 \end{bmatrix} = \underline{B} \ \underline{u}_{hi} \qquad\qquad v = \begin{bmatrix} B_1 & B_2 & B_3 \end{bmatrix} \begin{bmatrix} v_1 \\ v_2 \\ v_3 \end{bmatrix} = \underline{B} \ \underline{u}_{vi} \qquad (B23)$$

Equation (B8) can be written in variational form as follows:

$$\Phi = \frac{1}{2} \int_A \left[ \left( \frac{\partial p}{\partial x} \right)^2 + \left( \frac{\partial p}{\partial y} \right)^2 \right] dA - \int_A Qp \ dA \qquad (B24)$$

Assuming also a linear variation of pressure over the triangular element, the problem again reduces to the solution of Poisson's equation, where the right hand side of the resulting matrix equation can be expressed by a column vector $\underline{Q}$, as follows:

$$\underline{Q} = \rho \left[ \underline{u}_{hi}^t \ \underline{B}_x^t \ \underline{B}_x \ \underline{u}_{hi} - 2\underline{u}_{hi}^t \ \underline{B}_x^t \ \underline{B}_y \ \underline{u}_{vi} + \underline{u}_{vi}^t \ \underline{B}_y^t \ \underline{B}_y \ \underline{u}_{vi} \right] \qquad (B25)$$

After the pressure distributions around the airfoil are calculated, the lift and drag coefficients for the airfoil's unsteady pitching and plunging motion can be computed. When computed results are tabulated, the unsteady aerodynamic characteristics of airfoils for various flight conditions are readily evaluated.

### Accuracy and Stability of Solutions of the Vorticity Transport Equation

The numerical errors involved in the mathematical analysis of the vorticity transport equation can be summarized as computational errors and discretization errors. Both kinds of errors are closely related to the stability of the governing differential equations and can be analyzed in two parts:

- solution of the system of linear algebraic equations resulting from the finite element representation of Laplace's equation

- finite element formulation and numerical integration of the vorticity transport equation.

Errors involved in the solution of Laplace's equation. - The Lagrange multiplier technique used in the solution of Laplace's equation aids in understanding the errors involved in the analysis. Matrix $\underline{A}^*$ in

equation (A10) represents Laplace's equation over a rectangular grid with specified boundary conditions. This is equivalent to the finite element representation of the plane stress problem of a rectangular section. The accuracy of the solution has been discussed by various authors [ref. 23, 24]. The conditioning number for such a matrix is proportional to $n^2$, where n is the number of elements in the larger dimension of a rectangular grid. Consequently, for the grid used in the presented analysis, as shown in figure 3, satisfactory answers were obtained.

Errors involved in the numerical integration of the vorticity transport equation. - The numerical integration of the vorticity transport equation involved both computational and discretization errors. The accuracy of the numerical integration can be checked by using different numerical integration techniques and different integration step sizes. The results in figure 16 indicate that results obtained from the numerical method are stable for the chosen particular time step sizes, depending on the position of a point with respect to the airfoil boundary. In order to understand this behavior, an error analysis can be made on a typical triangular element of the grid in figure 3.

The Euler method was chosen in illustrating the stability of the numerical results because of its simplicity. The instability conditions for a steady flow case are analyzed by neglecting the effects of generalized unsteady forces on the airfoil boundary, since they decrease rapidly as the solution converges to a steady state. The vorticity transport equation can be written in matrix form as

$$\frac{\partial \underline{\omega}}{\partial t} = \underline{A}\,\underline{\omega} \qquad (B26)$$

From which, using a forward difference relationship one can write

$$\underline{\omega}_{n+1} = (\underline{I} + \underline{A}\,\Delta t)\underline{\omega}_n \qquad (B27)$$

Following Richtmeyer [ref. 22] the stability of equation (B17) can be determined by checking whether the following expression has a finite value:

$$\lim_{n \to \infty} \underline{\omega}_n = (\underline{I} + \underline{A}\,\Delta t)^n\,\underline{\omega}_0 \qquad (B28)$$

28

Since matrix $\underline{A}$ converges to a constant matrix, the changes in this matrix can be neglected for the steady state problem. The stability of equation (B17) can then be determined by checking whether the largest eigenvalue of

$$(\underline{I} + \underline{A}\, \Delta t) \leq 1$$

or                                                                                      (B29)

$$\Delta t \leq \frac{2}{\delta_{max}}$$

$\delta_{max}$ can be estimated from the finite element model by obtaining an upper bound for the largest eigenvalue of matrix $\underline{A}$. Since the system of equations is assembled from triangular elements [ref. 24]

$$\delta_{max} \overset{<}{-}\, \gamma_{max}$$                                                                  (B30)

where $\gamma_{max}$ is the maximum value of the eigenvalues of each triangular element. The problem then reduces to estimating the largest eigenvalue of a typical triangle from the following equation

$$\gamma_{i\ max} = \frac{\underline{\omega}_i^{t}\, \underline{A}_i\, \underline{\omega}_i}{\underline{\omega}_i^{t}\, \underline{\omega}_i}$$                                                                  (B31)

For a triangular element, with a linear variation of vorticity and velocity distribution, the largest eigenvalue can be calculated by substituting

$$\underline{\omega} = \underline{\omega}_o\, e^{-\gamma_i t}$$                                                                  (B32)

into the vorticity transport equation. Equation (B17) can be written in matrix form for each triangular element as follows:

29

$$\left\{ - \frac{\gamma_i A}{12} \begin{bmatrix} 2 & 1 & 1 \\ 1 & 2 & 1 \\ 1 & 1 & 2 \end{bmatrix} + \begin{bmatrix} \frac{\nu y_{23}}{4A} + \frac{1}{24}(2u_1 + u_2 + u_3) \\ \frac{\nu y_{31}}{4A} + \frac{1}{24}(u_1 + 2u_2 + u_3) \\ \frac{\nu y_{12}}{4A} + \frac{1}{24}(u_1 + u_2 + 2u_3) \end{bmatrix} \begin{bmatrix} y_{23} & y_{31} & y_{12} \end{bmatrix} \right.$$

$$\left. + \begin{bmatrix} \frac{\nu x_{32}}{4A} + \frac{1}{24}(2v_1 + v_2 + v_3) \\ \frac{\nu x_{13}}{4A} + \frac{1}{24}(v_1 + 2v_2 + v_3) \\ \frac{\nu x_{21}}{4A} + \frac{1}{24}(v_1 + v_2 + 2v_3) \end{bmatrix} \begin{bmatrix} x_{32} & x_{13} & x_{21} \end{bmatrix} \right\} \begin{bmatrix} \omega_{1o} \\ \omega_{2o} \\ \omega_{3o} \end{bmatrix} = \underline{0} \qquad (B33)$$

For a typical triangular element in figure 3, with base b and height h = 2b, the magnitude of the maximum eigenvalue $\gamma_i$ of an element will depend on the kinematic viscosity $\nu$ and the velocity distribution u and v. The stability of the solution for the vorticity distribution can be estimated from the largest eigenvalue of the system of equation (B33) for several typical cases.

For a triangular element in the free stream, where u is constant and v = 0, the eigenvalues do not depend on the velocity distribution. The largest eigenvalue then becomes

$$\gamma_i = \frac{25.8\nu}{h^2} \qquad (B34)$$

As can be seen from equation (B34), when the viscosity terms are neglected, the numerical integration of the inviscid flow equations becomes infinitely stable for the free stream flow. The importance of the velocity terms, however, is apparent at the triangles on the boundary of an obstacle. Assuming a triangle with a base on the airfoil boundary ($u_1 = u_3 = 0$) and neglecting the vertical velocities ($v_1 = v_2 = v_3 = 0$), the largest eigenvalue of equation (B33) can be written as

$$\gamma_i = 15 \left(\frac{\nu}{h^2}\right) + \sqrt{117 \left(\frac{\nu}{h^2}\right)^2 - 6\left(\frac{\nu}{h^2}\right) \left(\frac{u_2}{h}\right)} \tag{B35}$$

The stability of equation (B26) depends on the real part of the $\gamma_i$ in equation (B35). If the velocity term $u_2$ satisfies equation (B36),

$$u_2 < 19.5 \frac{\nu}{h} \tag{B36}$$

then $\gamma_i$ is a real number and the time step of the numerical integration can be estimated from equation (B36) as an upper bound. However, if equation (B36) is not satisfied, then the numerical integration will have an oscillatory convergence. Also, equation (B36) shows that at the boundary layer region, where the velocity distribution varies parabolically starting from the airfoil boundary, stable results can be obtained by using smaller triangles and decreasing $u_2$ for the triangles at the boundary of the airfoil.

# REFERENCES

1. Amsden, A. A., and Harlow, F. H.: The SMAC Method: A Numerical Technique for Calculating Incompressible Fluid Flows. Los Alamos Scientific Laboratory Report LA-4370, May 1970.

2. Cheng, S. I.: Numerical Integration of Navier-Stokes Equations. AIAA J., Vol. 8, No. 12, Dec. 1970, p. 2115.

3. Fromm, J. E.: A Method for Computing Nonsteady, Incompressible, Viscous Fluid Flows. Los Alamos Scientific Laboratory Report LA-2910, Sept. 1963.

4. Gentry, R. A., Martin, R. E., and Daly, B. J.: An Eulerian Differencing Method for Unsteady Compressible Flow Problems. J. Computational Phys., Vol. 1, No. 1, July 1966, p. 87.

5. Harlow, F. H.: Numerical Methods for Fluid Dynamics, An Annotated Bibliography. Los Alamos Scientific Laboratory Report LA-4281, Dec. 1970.

6. Roache, P. J., and Mueller, T. J.: Numerical Solutions of Laminar Separated Flows. AIAA J., Vol. 8, No. 3, March 1970, p. 530.

7. Dwyer, H. A.: Solution of a Three-Dimensional Boundary-Layer Flow with Separation. AIAA J., Vol. 6, No. 7, July 1968, p. 1336.

8. Dwyer, H. A., and McCroskey, W. J.: Crossflow and Unsteady Boundary-Layer Effects on Rotating Blades. AIAA Paper No. 70-50, AIAA 8th Aerospace Sciences Meeting, New York, Jan. 19-21, 1970.

9. Hicks, J. G., and Nash, J. F.: The Calculation of Three-Dimensional Turbulent Boundary Layers on Helicopter Rotors. NASA-CR-1845, May 1971.

10. Bowley, W. W., and Prince, J. F.: Finite Element Analysis of General Fluid Flow Problems. AIAA Paper No. 71-602, AIAA 4th Fluid and Plasma Dynamics Conference, June 21-23, 1971.

11. Hess, J. L., and Smith, A.M.O.: Calculation of Potential Flow About Arbitrary Bodies. Progress in Aeronautical Sciences, Vol. 8, Pergamon Press, 1967, p. 1.

12. Oden, J. T., and Somogyi, D.: Finite-Element Applications in Fluid Dynamics. J. ASCE, Eng. Mechs. Div., Vol. 95, EM 3, June 1969, p. 821.

13. Skalak, R., Zarda, P. R., Chen, P. H., and Chen, T. C.: A Variational Principle for Slow Viscous Flow with Suspended Particles. Proc. of the Symp. on Computer Aided Engineering, held at the Univ. of Waterloo, May 11-13, 1971, G.M.L. Gladwell, ed., p. 471.

14. Tong, P.: The Finite Element Method for Fluid Flow Analysis. Recent Advances in Matrix Methods of Structural Analysis and Design, R. H. Gallagher, Y. Yamada, and J. T. Oden, eds., The Univ. of Alabama Press, Alabama, 1971, p. 787.

15. Lemieux, P. F., Unny, T. E., and Dubey, R. N.: Variational Principle in Fluid Dynamics. J. ASCE, Eng. Mechs. Div., EM 6, Dec. 1970, p. 1031.

16. Glansdorff, P., and Prigogine, I.: On a General Evolution Criterion in Macroscopic Physics. Physica 30, 1964, p. 351.

17. Zienkiewicz, O. C.: The Finite Element Method in Structural and Continuum Mechanics. McGraw-Hill Publishing Company, Limited, Great Britain, 1967.

18. Harlow, F. H., Dickman, D. O., Harris, D. E. Jr., and Martin, R. E.: Two-Dimensional Hydrodynamic Calculations. Los Alamos Scientific Laboratory Report LA-2301, Sept. 1959.

19. Houghton, E. L., and Boswell, R. P.: Further Aerodynamics for Engineering Students. St. Martin's Press, New York, 1969.

20. Mikhlin, S. G.: Variational Methods in Mathematical Physics. The Macmillan Co., New York, 1964.

21. Ecer, A.: Finite Element Analysis of Post-Buckling Behaviour. Ph.D. Dissertation, Univ. of Notre Dame, Jan. 1970.

22. Richtmeyer, R. D.: Difference Methods for Initial-Value Problems. Interscience Publishers, Inc., New York, 1957.

23. Kelsey, S., Lee, K. N., and Mak, C.K.K.: The Condition of Some Finite Element Coefficient Matrices. Proc. of the Symp. on Computer Aided Engineering, held at the Univ. of Waterloo, 1971, G.M.L. Gladwell, ed., p. 267.

24. Tong, P.: On the Numerical Problems of the Finite Element Methods. Proc. of the Symp. on Computer Aided Engineering, held at the Univ. of Waterloo, 1971, G.M.L. Gladwell, ed., p. 539.

| Reynolds Number | Angle of Attack | Number of Integration Steps Required to Obtain a Steady State | C.P.U. Time |
|---|---|---|---|
| 1000 | 4 | 140 | 9.1 min |
| 1000 | 8 | 140 | 10.1 min |
| 105 | 4 | 75 | 5.0 min |
| 105 | 8 | 76 | 6.5 min |

Table 1.  Computer Time Required for the Solution
of Vorticity Transport Equation

```
┌─────────────────┐     ┌─────────────────┐     ┌─────────────────┐
│ input data air- │     │ mathematical    │     │ velocity        │
│ flow motion and │ ──► │ model           │ ──► │ distribution    │
│ flow            │     │ potential flow  │     │ streamfunctions,│
│ characteristics │     │ or unsteady     │     │ and velocities  │
│                 │     │ viscous flow    │     │ at each node    │
└─────────────────┘     └─────────────────┘     └─────────────────┘
```

```
        ┌─────────────────────┐     ┌──────────────┐
  ──►   │ computer graphics    │ ──► │ computer-    │
        │ package for          │     │ drawn        │
        │ generating movies    │     │ movies       │
        │ and illustrations    │     │              │
        └─────────────────────┘     └──────────────┘
```
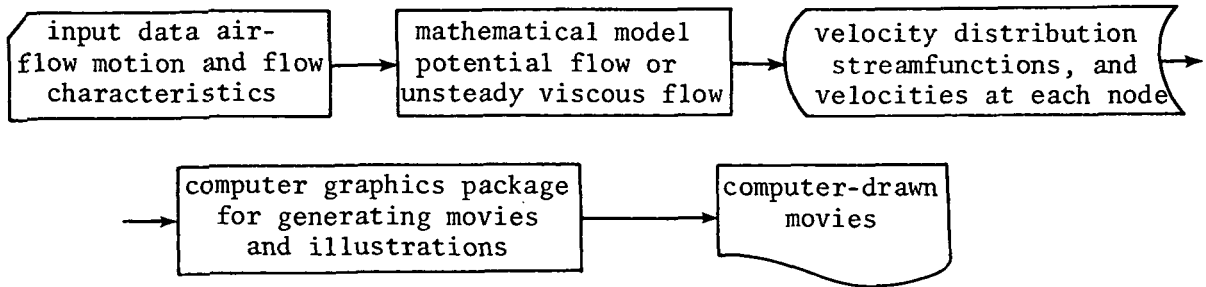
Fig. 1a.  Flow chart of the computer program for the mathematical analysis and visualization of flow around oscillating airfoils

```
┌──────────┐     ┌─────────────────┐     ┌──────────────┐
│ input    │ ──► │ solution of     │ ──► │ velocity     │
│ data     │     │ Poisson's       │     │ distribution │
│          │     │ equation        │     │              │
└──────────┘     └─────────────────┘     └──────────────┘
```

Potential Flow

```
   ┌──────────────────────────────────────────────────────────────┐
   │                                                                │
┌──────┐  ┌───────────┐  ┌──────────────┐  ┌───────────┐  ┌──────────────┐
│input │─►│ velocity  │─►│ solution of  │─►│ velocity  │─►│ integration  │─┐
│data  │  │distribution│  │ Poisson's   │  │distribution│  │ of vorticity │ │
│      │  │           │  │ equation     │  │           │  │ transport    │ │
│      │  │           │  │              │  │           │  │ equations    │ │
└──────┘  └───────────┘  └──────────────┘  └───────────┘  └──────────────┘ │
                                                                            │
```

Unsteady Viscous Flow
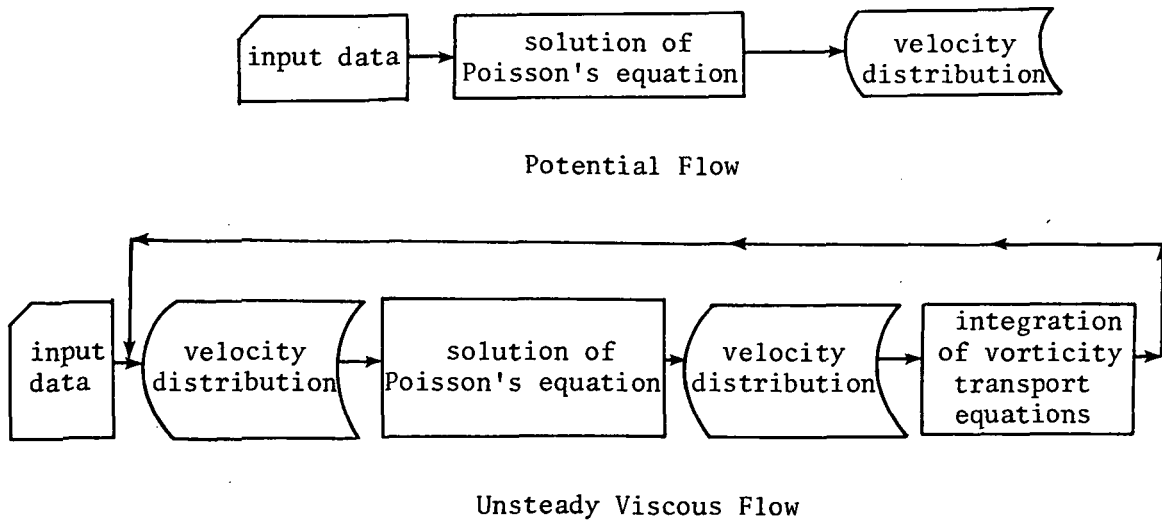
Fig. 1b.  Flow chart of the program for the solution of the flow around an oscillating airfoil from potential flow and the vorticity transport equation

```
┌──────────────┐         ┌────────────────────────────┐         ┌──────────────────┐
│  velocity    │────────▶│  numerical integration     │────────▶│   motion of      │────▶
│ distribution │         │  of velocity distribution  │         │  fluid particles │
└──────────────┘         │  to determine streamlines, │         └──────────────────┘
                         │  streaklines and pathlines │
                         └────────────────────────────┘

        ┌───────────────────────────────┐         ┌──────────────────┐
───────▶│  computer graphics routines   │────────▶│ computer-drawn    │
        │  for generating illustrations │         │     movies        │
        │          and movies           │         └──────────────────┘
        └───────────────────────────────┘
```
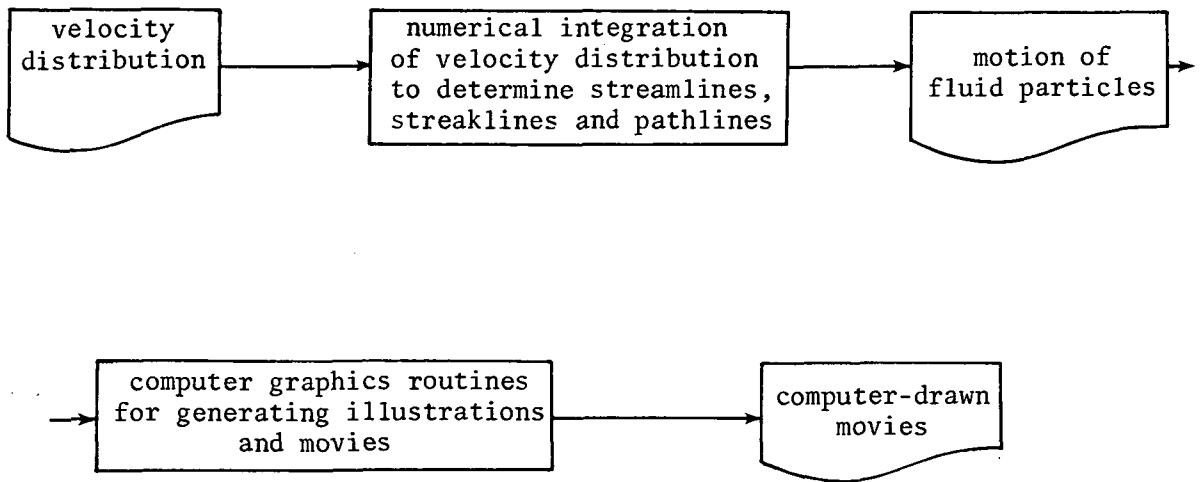
Fig. 1c.  Flow chart of the program for generating computer-drawn
movies from the output of the flow analysis
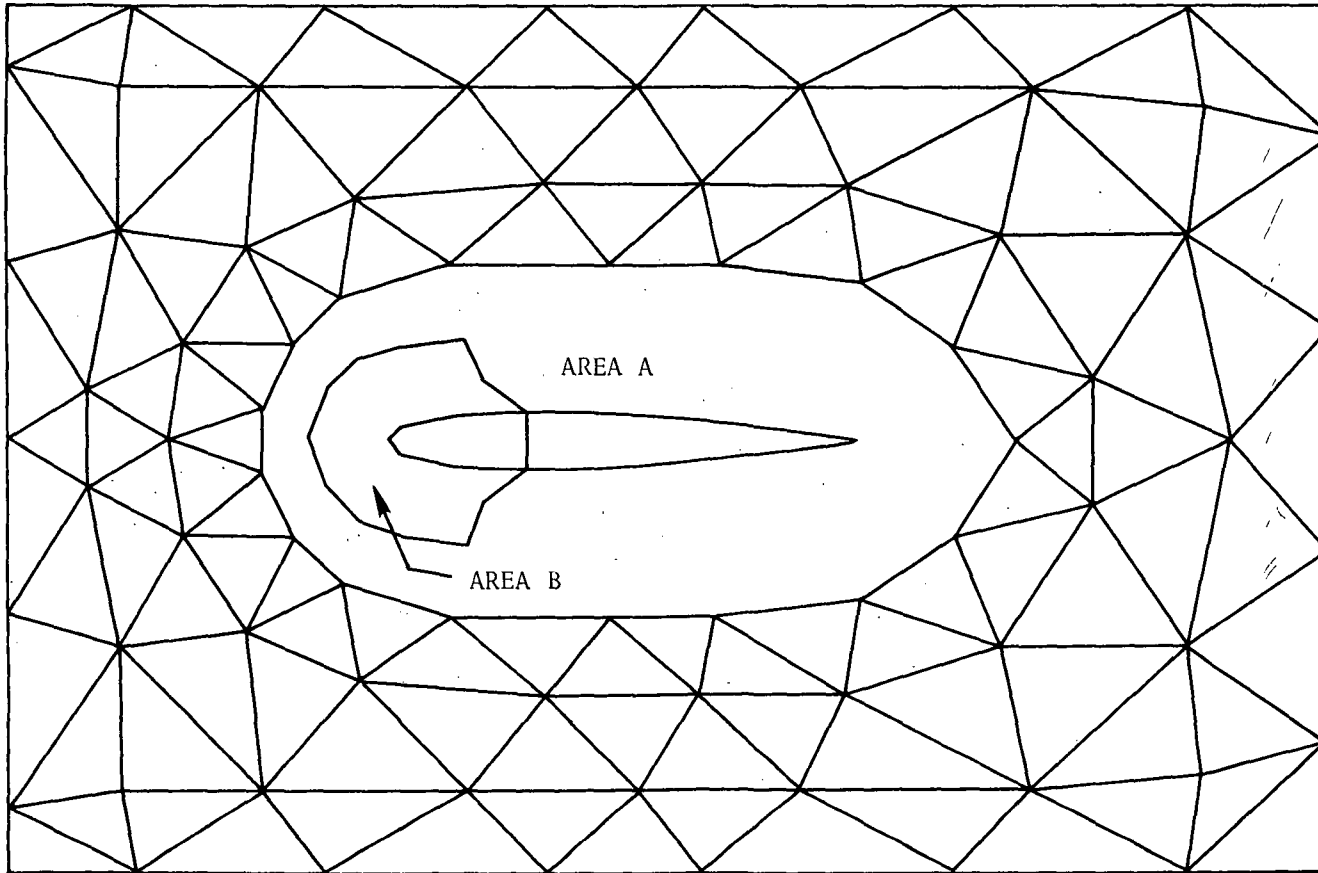
Fig. 2a.  Finite Element Gridwork
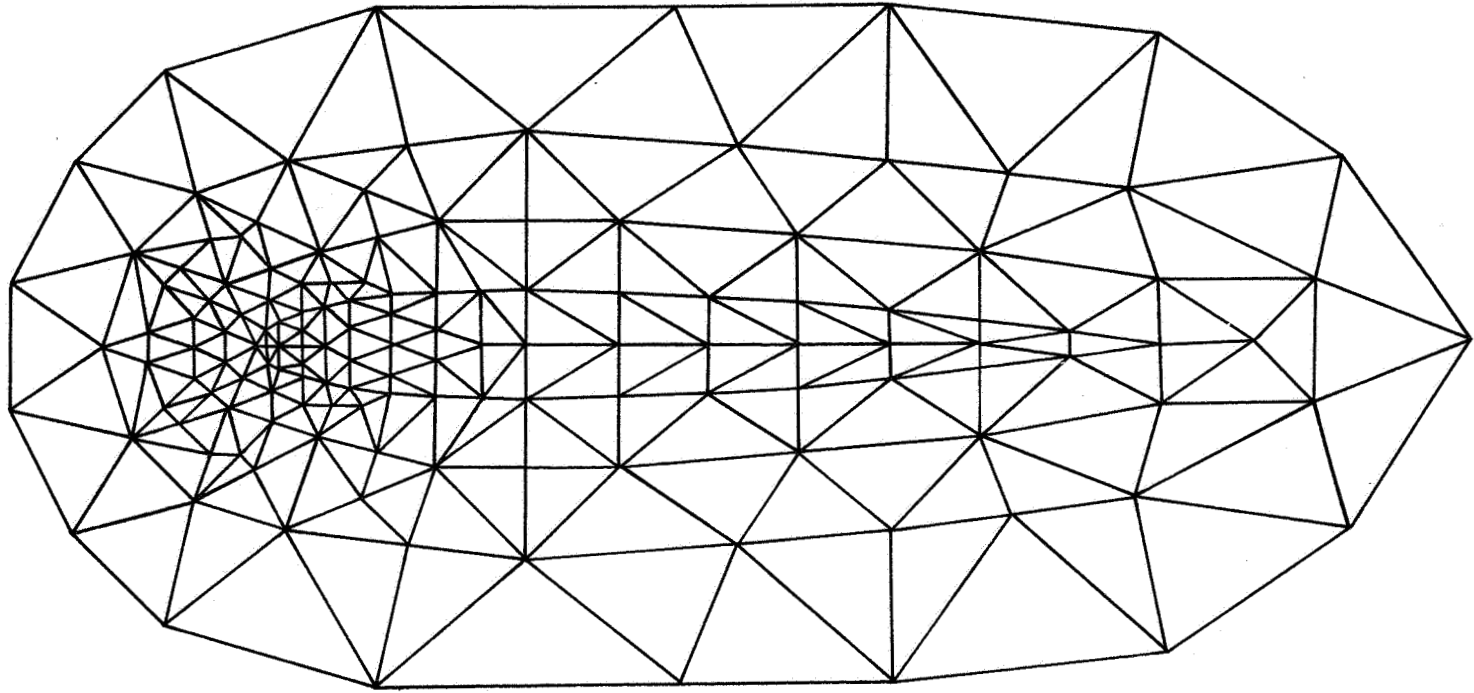
Fig. 2b.   Finite Element Gridwork for Area A
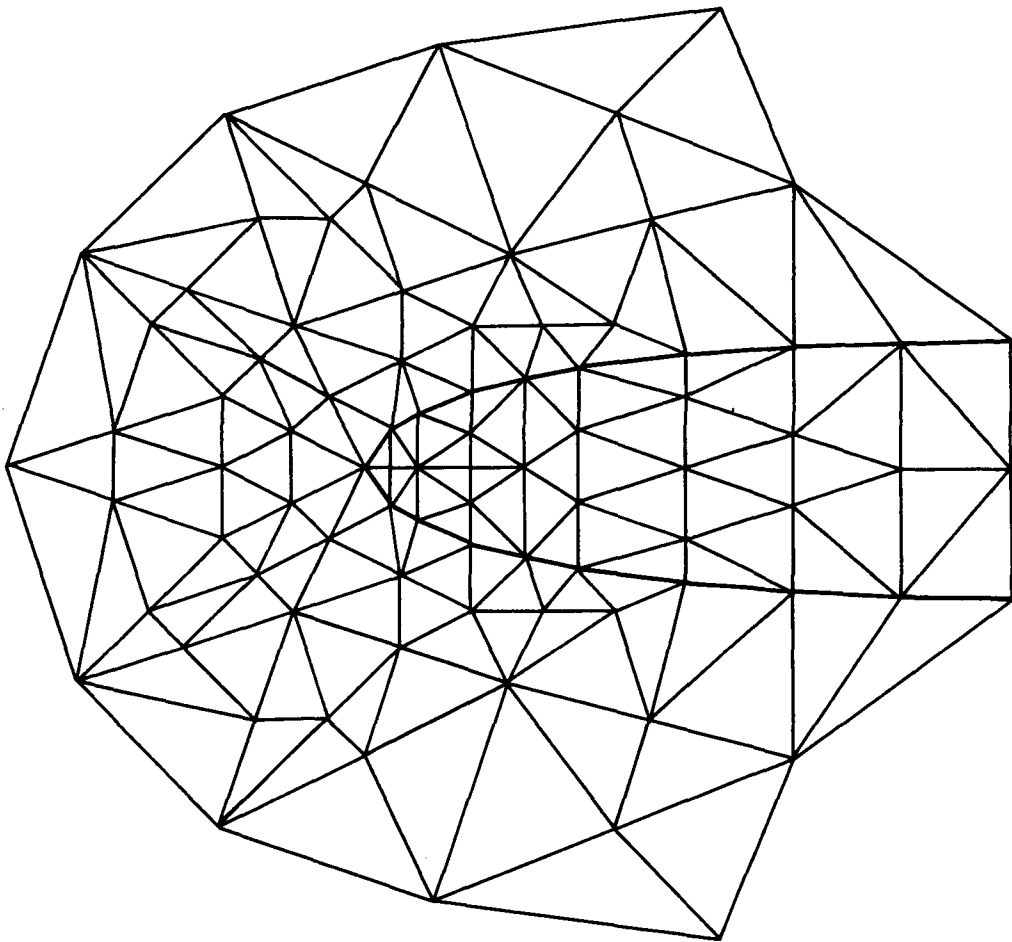
Fig. 2c.   Finite Element Gridwork for Area B
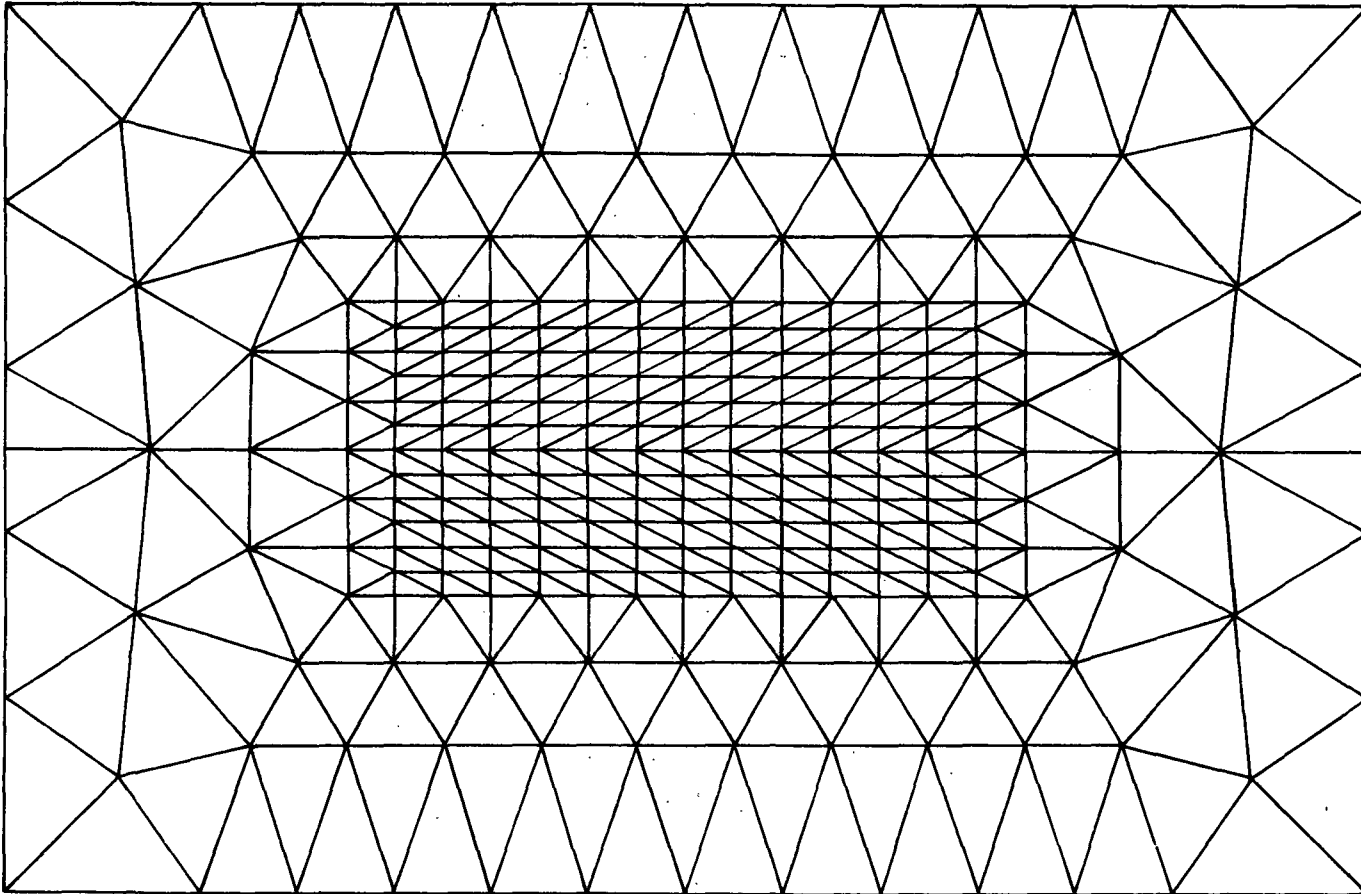
Fig. 3.  Complete Finite Element Gridwork for the Unsteady Viscous Flow Problem
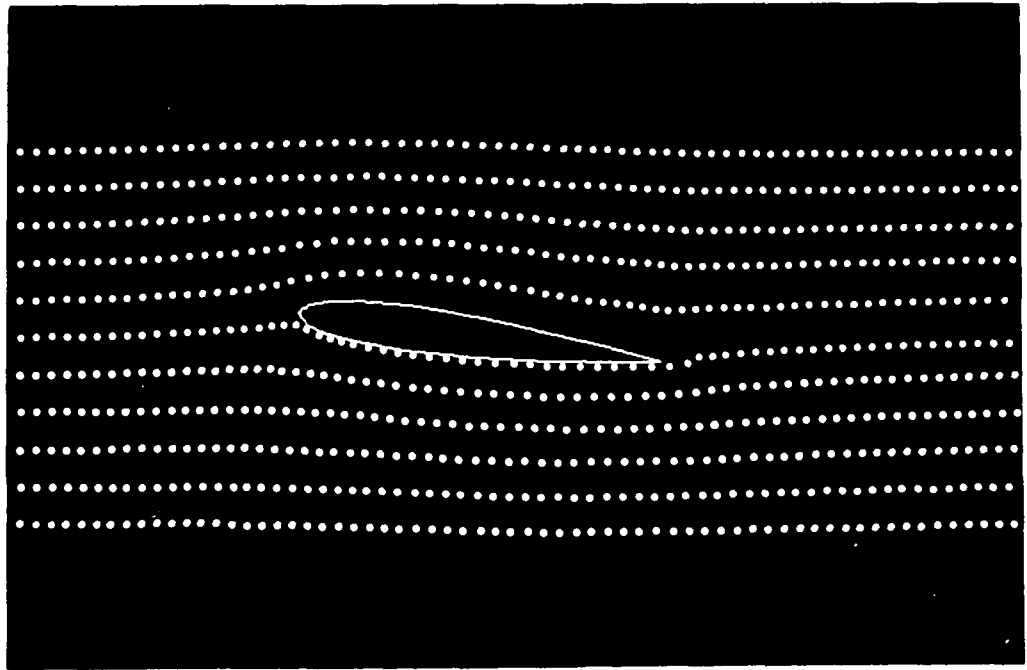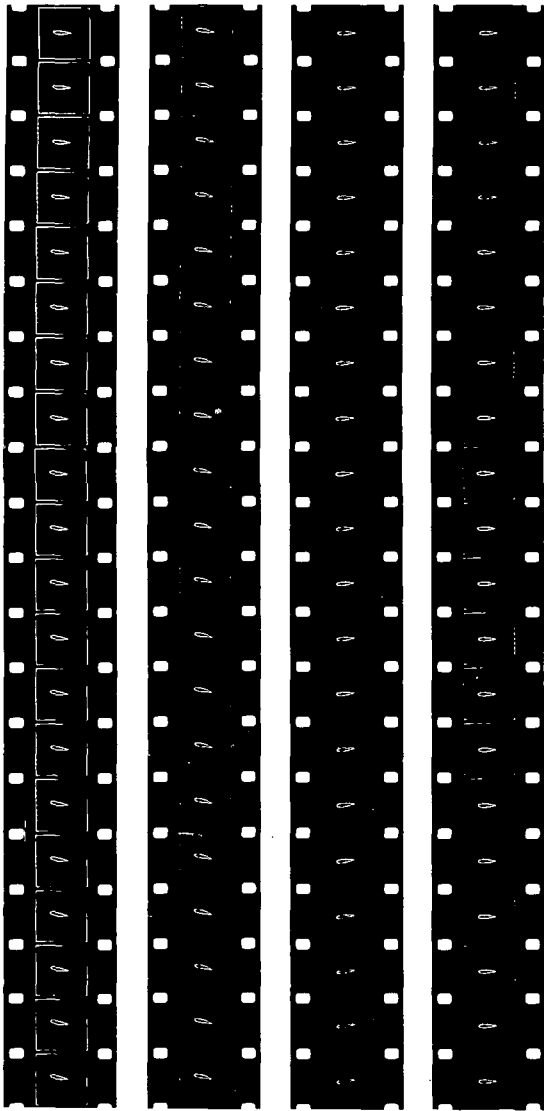
Fig. 4a.  Sample frames from a computer-drawn movie showing the flow of air particles around a pitching and plunging NACA 0012 airfoil. The mathematical model used for the preparation of the movie was based on potential flow theory. Each frame represents location of air particles at 1/24 second time intervals.
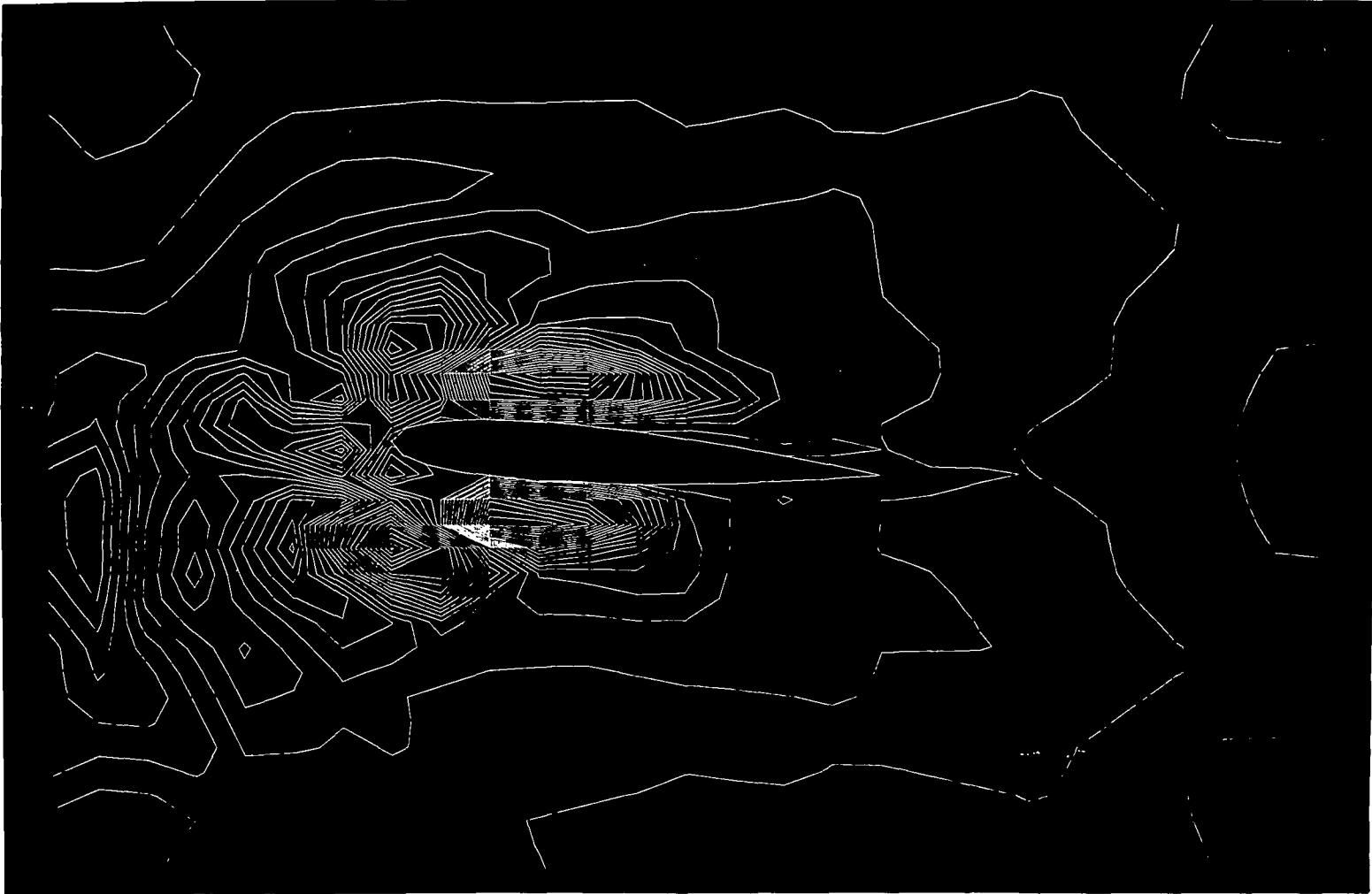
Fig. 4b.  Sample computer-drawn illustration showing details
of vorticity distribution around NACA 0012 airfoil
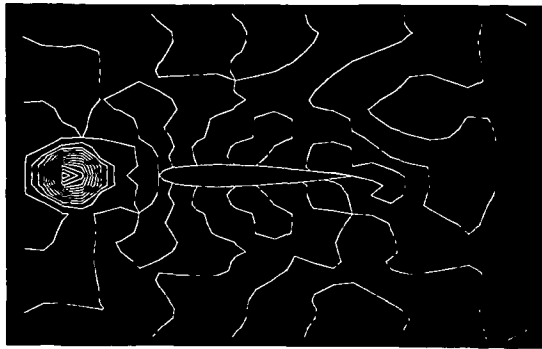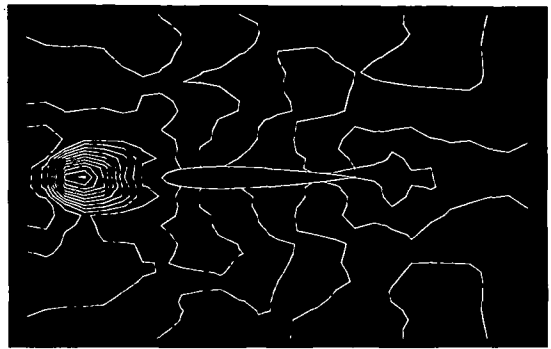
t = 0.1 sec.　　　　　　　　t = 1.2 sec.

t = 2.4 sec.　　　　　　　　t = 4.8 sec.
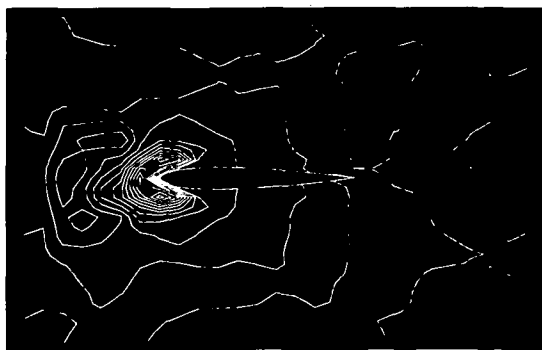
t = 6.0 sec.　　　　　　　　t = 7.2 sec.
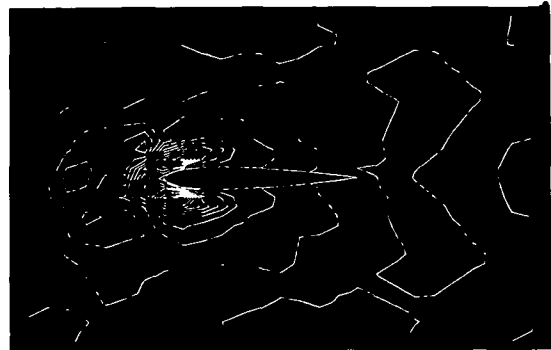
Fig. 5a. Vorticity distribution around a NACA 0012 airfoil.
(Re = $10^3$, α = 0°) A vortex approaches and strikes the
airfoil, starting from a position of 47% chordwidth ahead
of the airfoil and separates into two vortices.  The
maximum vorticity on the vortex is initially equal to unity.

43
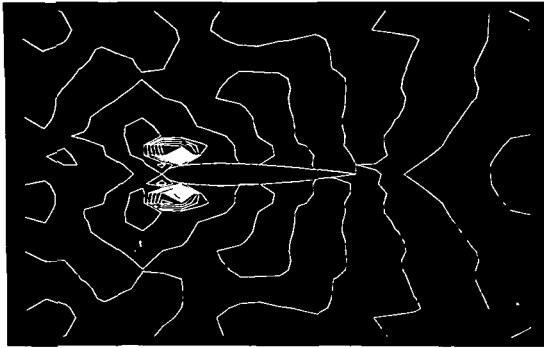
t = 0.1 sec.                    t = 0.8 sec.
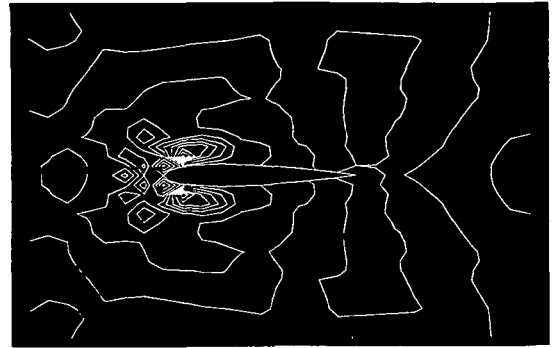
t = 1.6 sec.                    t = 2.4 sec.
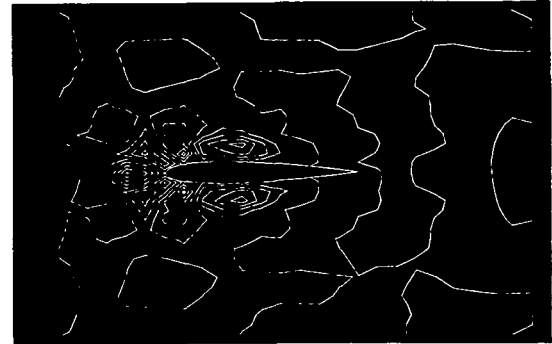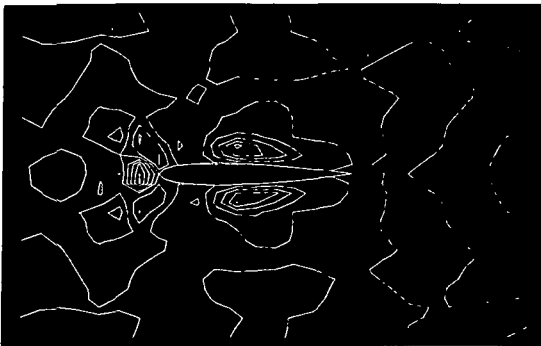
t = 3.2 sec.                    t = 4.0 sec.
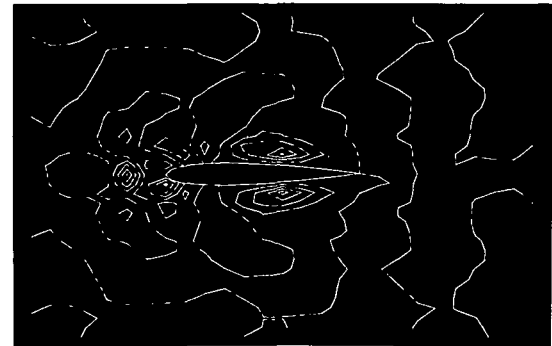
Fig. 5b. Vorticity distribution around a NACA 0012 airfoil.
(Re = $10^3$, $\alpha$ = 0°). The vorticity transport equations were
integrated with respect to time to obtain steady state
conditions; starting from an arbitrary vorticity distribution
i.e. two vortices, one below and one above the airfoil.
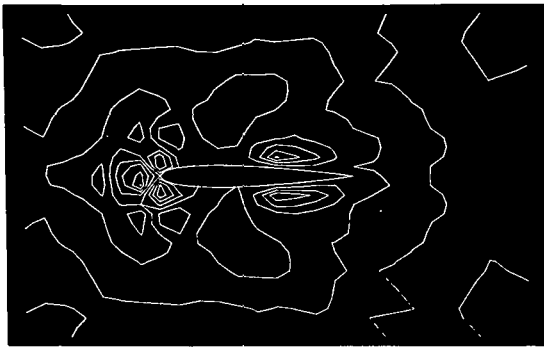
t = 4.8 sec.
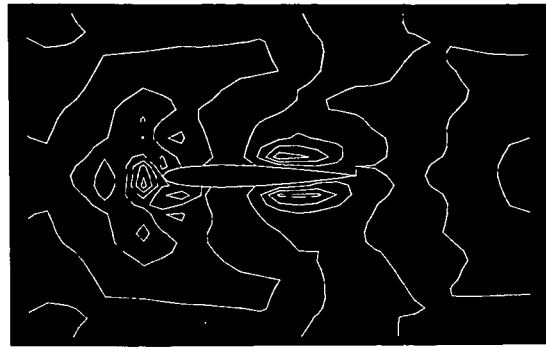
t = 5.2 sec.
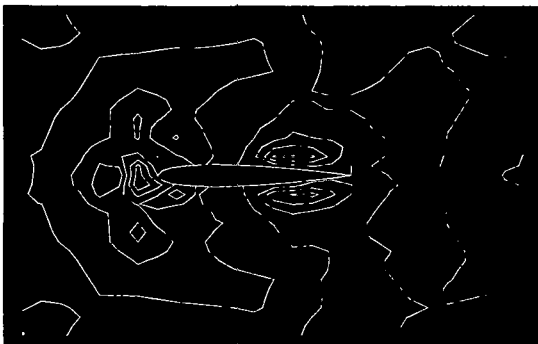
t = 5.6 sec.
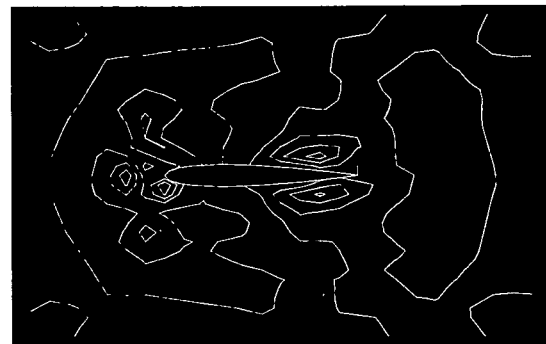
t = 6.4 sec.
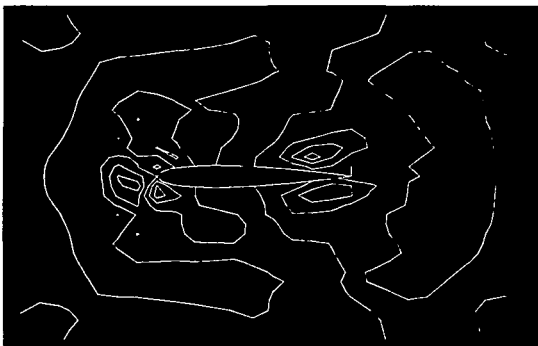
t = 7.2 sec.
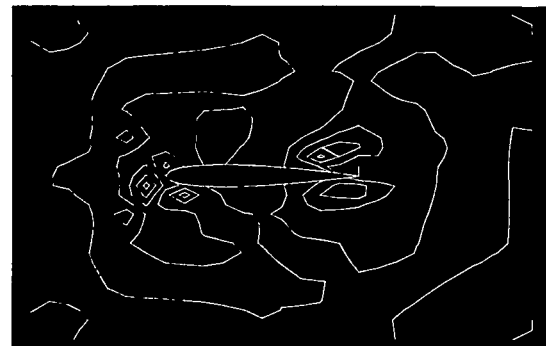
t = 8.0 sec.

Fig. 5c. Vorticity distribution around a NACA 0012 airfoil.
(Re = $10^3$, $\alpha$ = 0°). Two vortices, advancing along the airfoil,
converge to a steady state condition. Last frame shows the
vortices at trailing and leading edges of the airfoil for
steady state conditions.
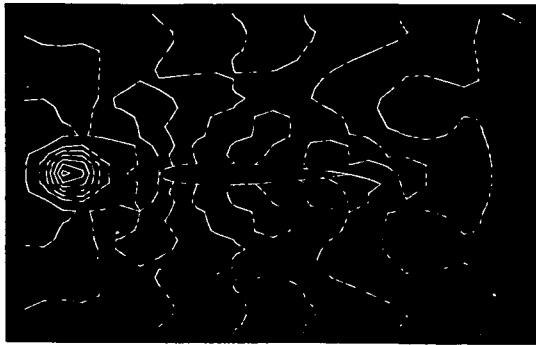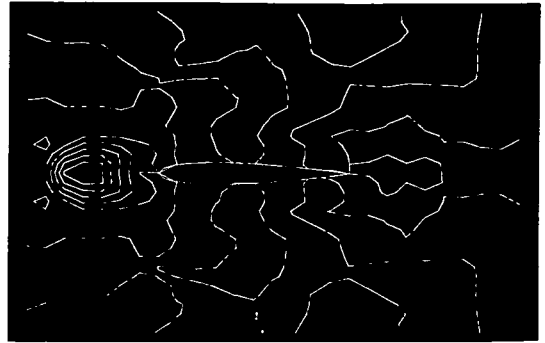
t = 0.002 sec.          t = 0.016 sec.
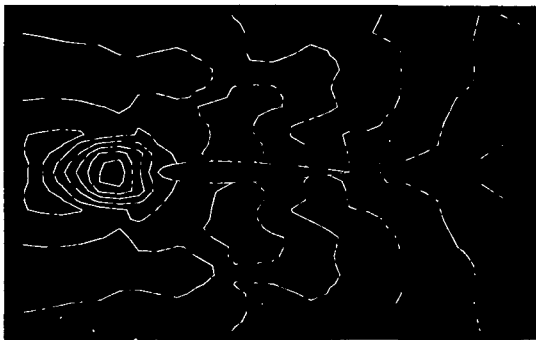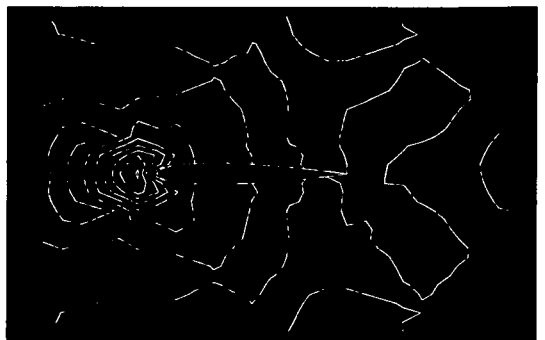
t = 0.032 sec.          t = 0.048 sec.

t = 0.064 sec.          t = 0.080 sec.
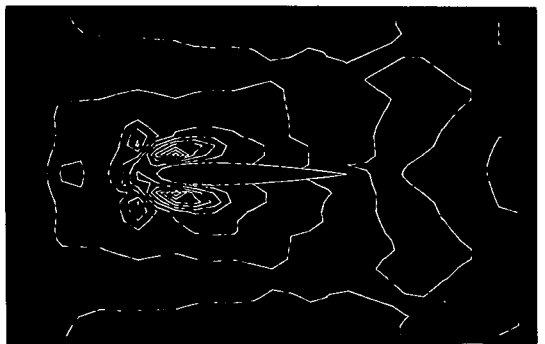
Fig. 6a. Vorticity distribution around a NACA 0012 airfoil.
$(Re = 10^5, \alpha = 0°)$. A unit vortex, as in Fig. 5a, advances
and strikes the airfoil. Compared to conditions at lower
Reynolds numbers, the maximum vorticities are travelling
closer to the airfoil.

46

t = 0.096 sec.
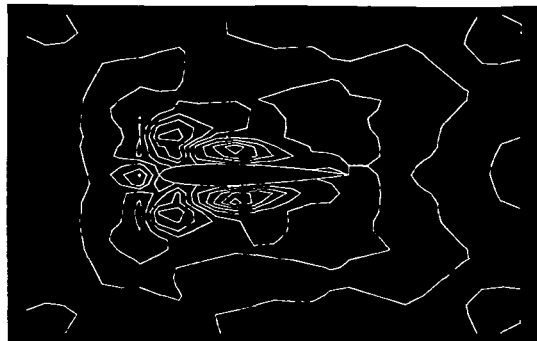
t = 0.112 sec.
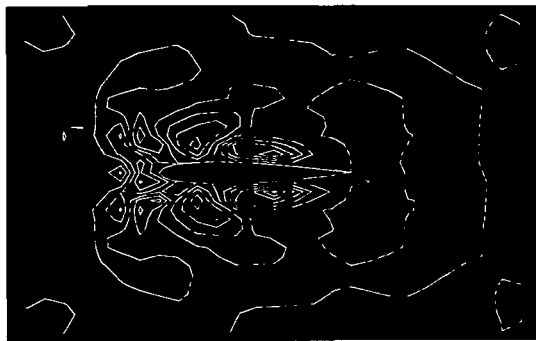
t = 0.128 sec.
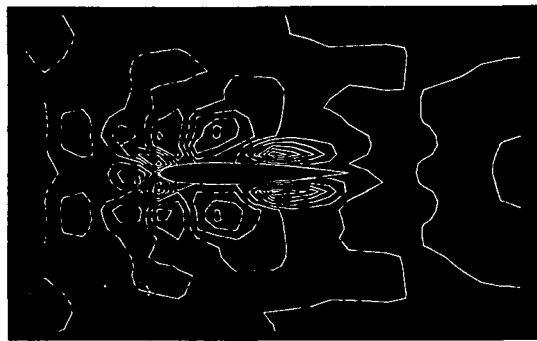
t = 0.144 sec.

t = 0.160 sec.

t = 0.176 sec.

Fig. 6b. Vorticity distribution around a NACA 0012 airfoil.
(Re = $10^5$, $\alpha$ = 0°).   As two vortices advance along the airfoil,
the magnitude of the vorticities at the leading edge of the
airfoil increase.  The vorticity distribution is relatively
unstable at the leading edge.

47
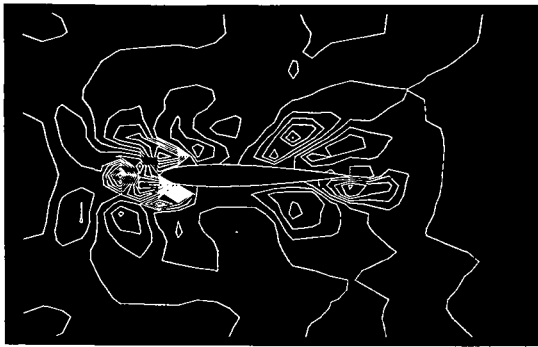
t = 0.192 sec.
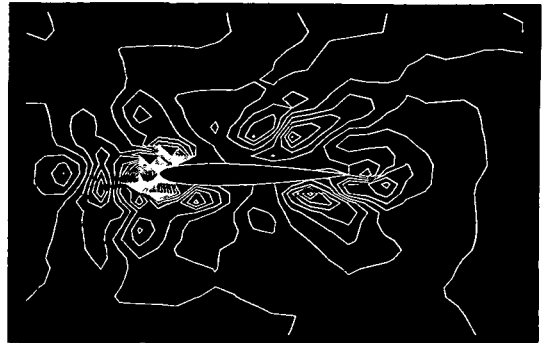
t = 0.208 sec.
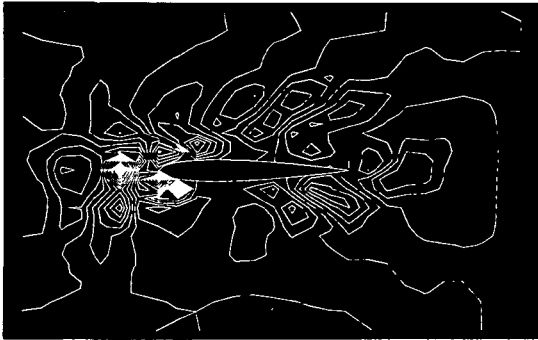
t = 0.224 sec.
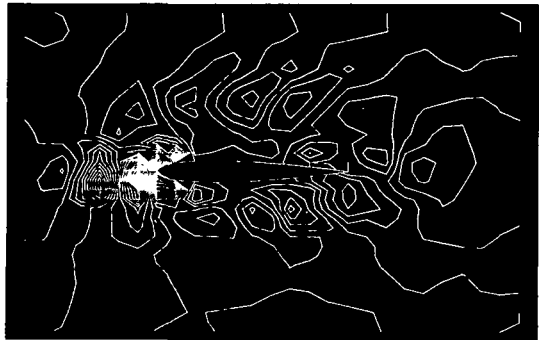
t = 0.240 sec.
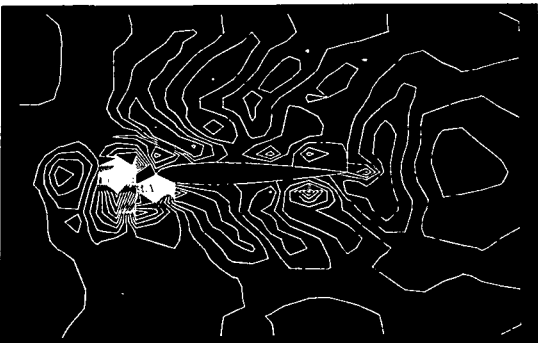
t = 0.256 sec.
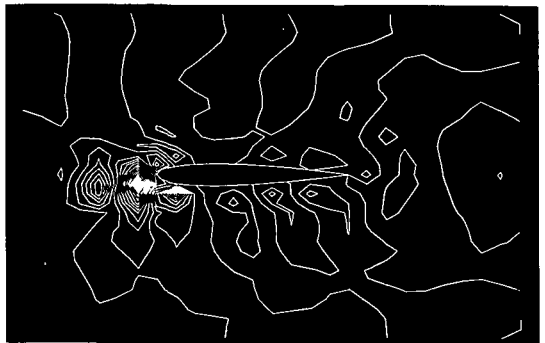
t = 0.272 sec.

Fig. 6c. Vorticity distribution around a NACA 0012 airfoil.
(Re = $10^5$, $\alpha$ = 0°). As the vorticity distribution around the
airfoil reaches a steady state at the trailing edge, at the
leading edge it is still unsteady. The last frame, for
t = 0.272 sec., is drawn at a larger scale and shows that
the vortex rings are distributed along the airfoil rather
than concentrated at the trailing edge, as in Fig. 5c.
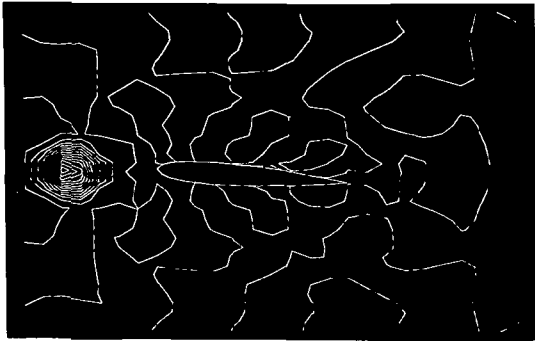
t = 0.1 sec.
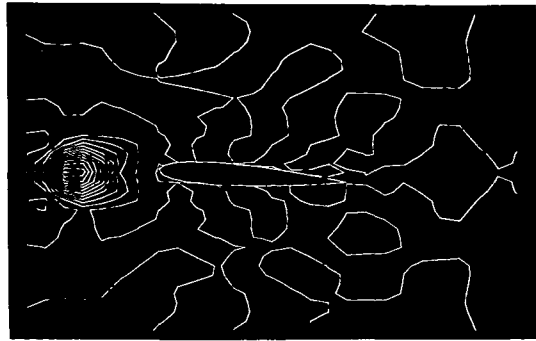
t = 0.8 sec.
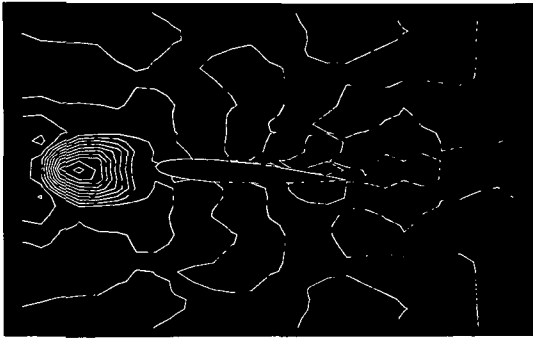
t = 1.6 sec.
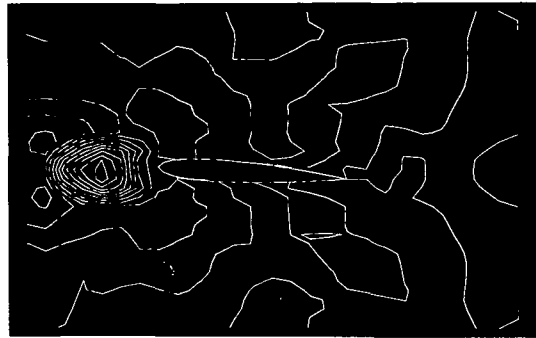
t = 2.4 sec.
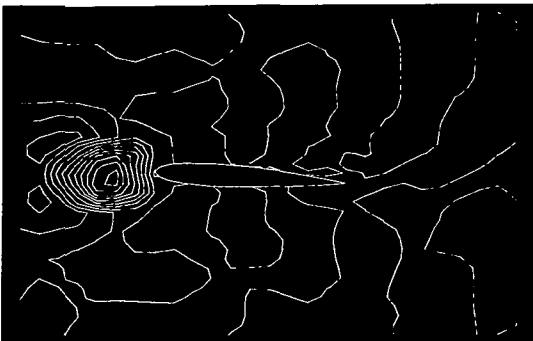
t = 3.2 sec.
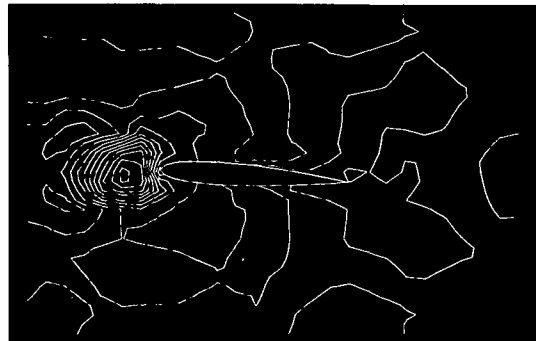
t = 4.0 sec.

Fig. 7a. Vorticity distribution around a NACA 0012 airfoil. (Re = $10^3$, $\alpha$ = 4°). A unit vortex, similar to the one in Fig. 5a, strikes the pitched airfoil.
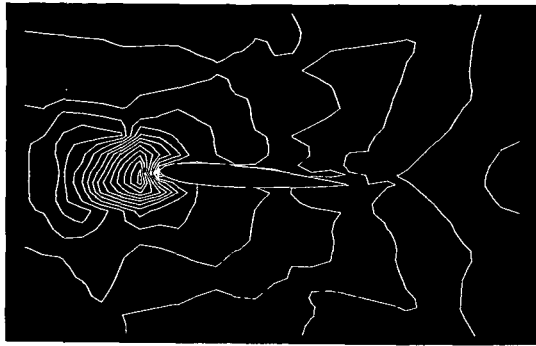
t = 4.8 sec.
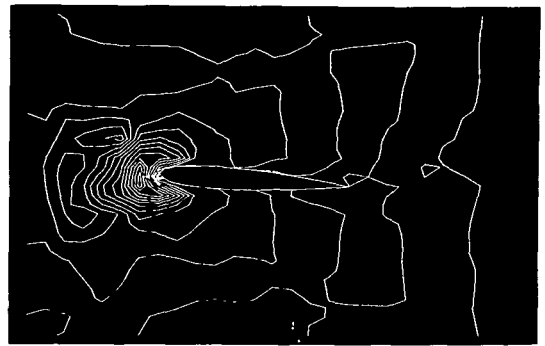
t = 5.6 sec.

t = 6.4 sec.

t = 7.2 sec.
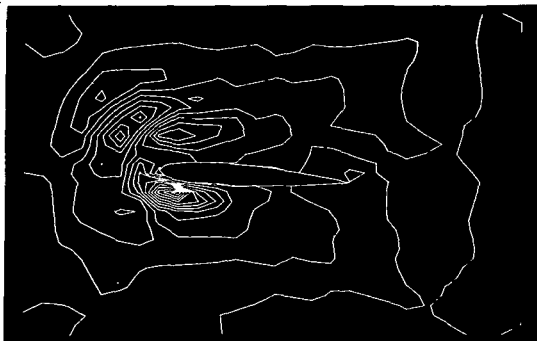
t = 8.0 sec.
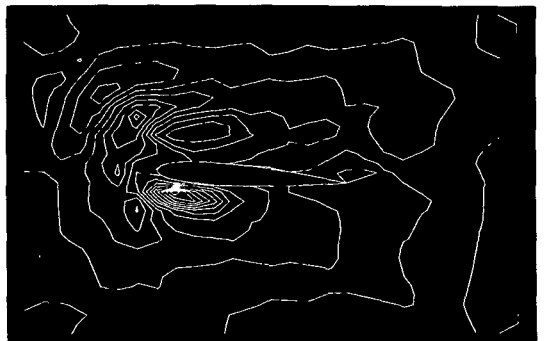
t = 8.8 sec.

Fig. 7b. Vorticity distribution around a NACA 0012 airfoil. (Re = $10^3$, $\alpha$ = 4°). The initial unit vortex separates into two asymmetric vortices; upper vortex moves away from the airfoil while lower one reaches a maximum vorticity near the airfoil.
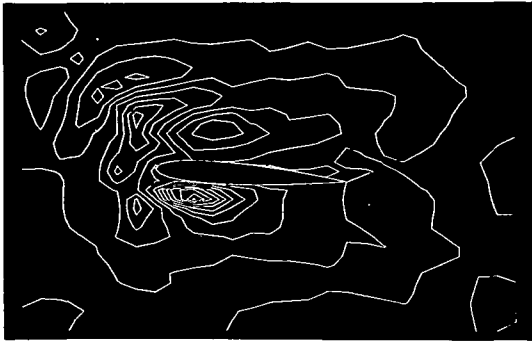
t = 9.6 sec.
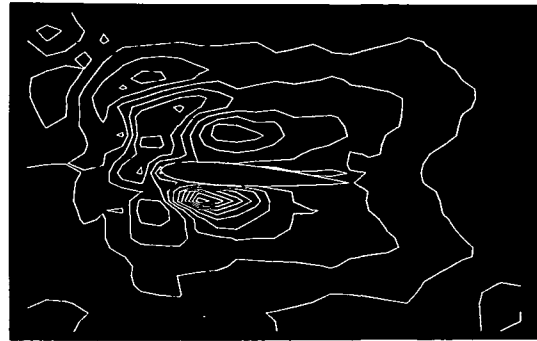
t = 10.4 sec.
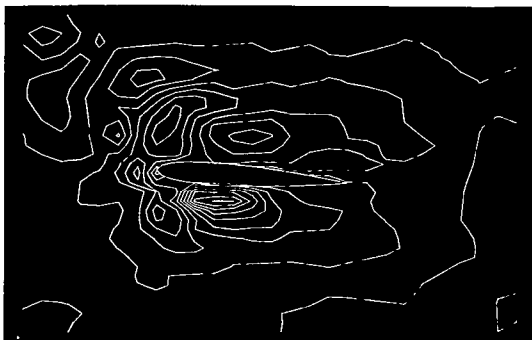
t = 11.2 sec.
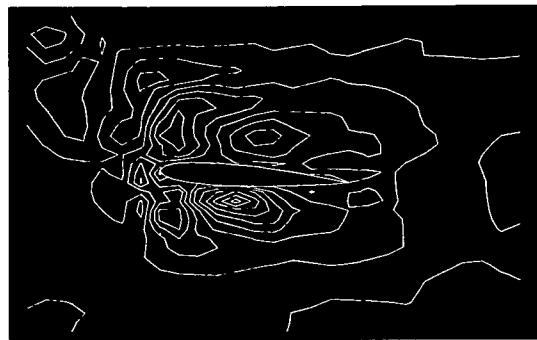
t = 12.0 sec.
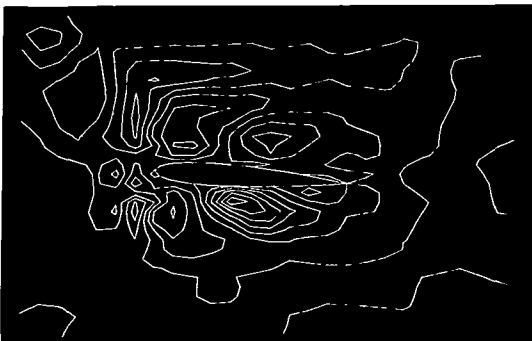
t = 12.8 sec.

t = 13.6 sec.

Fig. 7c. Vorticity distribution around a NACA 0012 airfoil.
(Re = $10^3$, $\alpha$ = 4°).  The numerical integration procedure was
continued until a steady state distribution was obtained.
Compared to Fig. 5c, these vortices are more evenly
distributed along the airfoil and closer to the leading
edge.  Beneath the airfoil the vortices adhere closer
to the surface and are larger in magnitude.
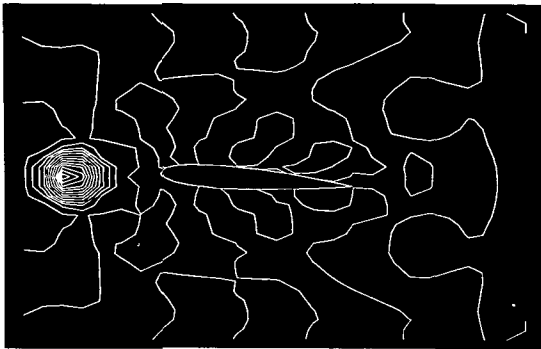
t = 0.002 sec.
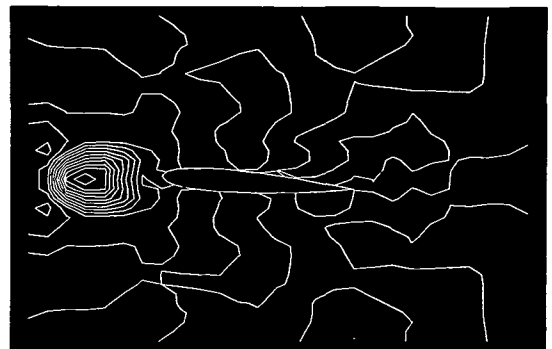
t = 0.016 sec.
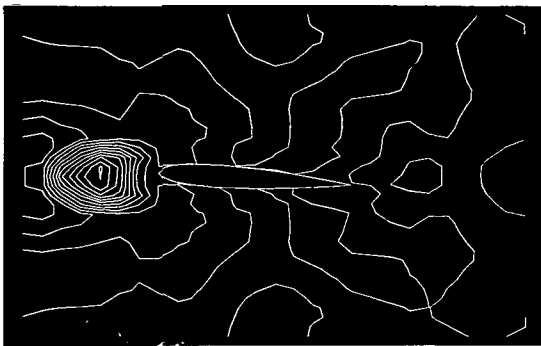
t = 0.024 sec.
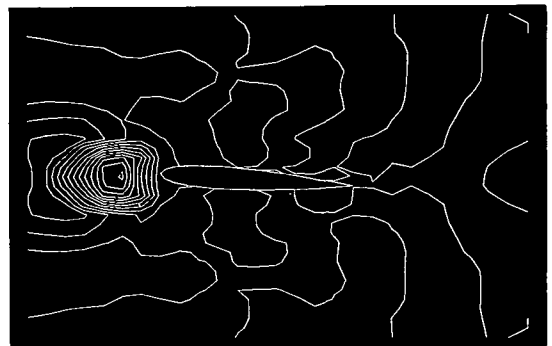
t = 0.032 sec.
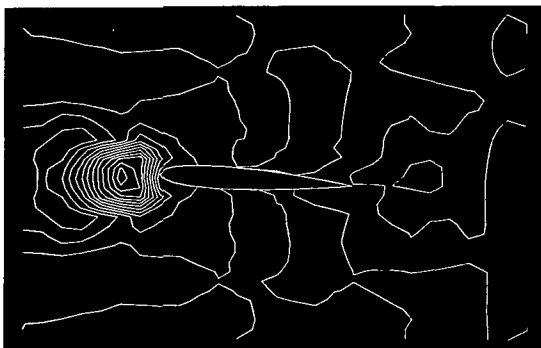
t = 0.040 sec.
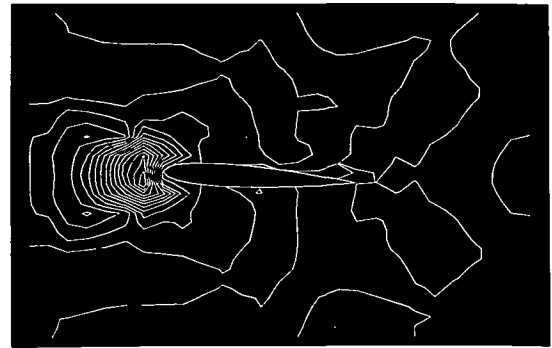
t = 0.048 sec.

Fig. 8a. Vorticity distribution around a NACA 0012 airfoil.
(Re = $10^5$, $\alpha$ = 4°). A unit vortex, similar to the one in
Fig. 6a, strikes the pitched airfoil.

52
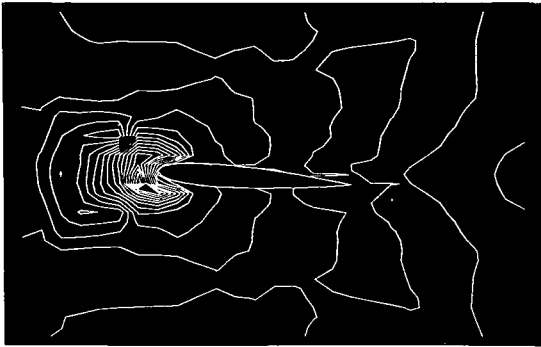
t = 0.056 sec.
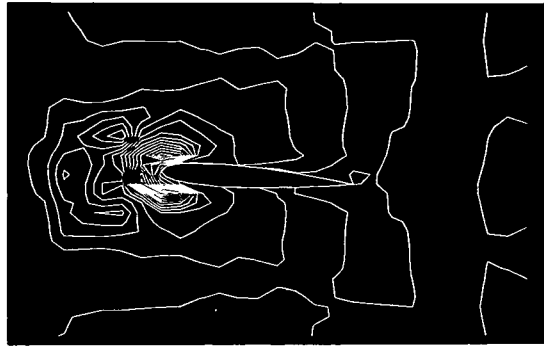
t = 0.064 sec.
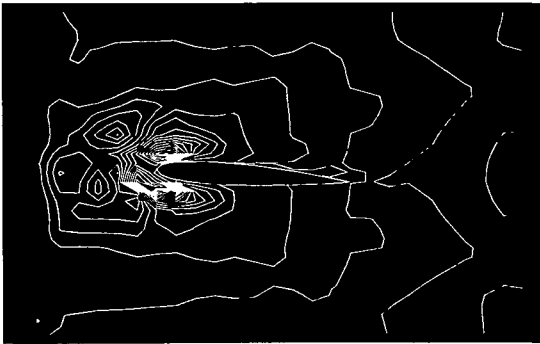
t = 0.072 sec.
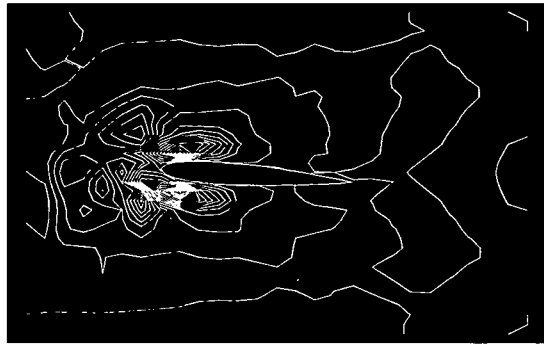
t = 0.080 sec.
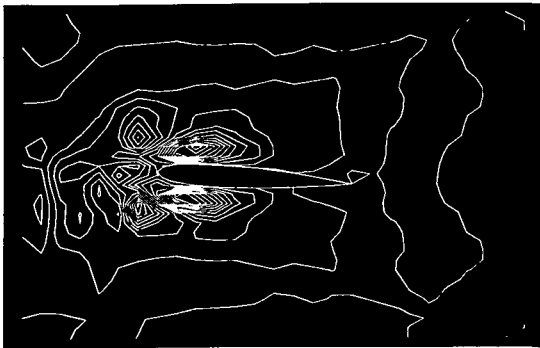
t = 0.088 sec.

t = 0.096 sec.

Fig. 8b. Vorticity distribution around a NACA 0012 airfoil. $(Re = 10^5, \alpha = 4°)$. The vortex separates and advances along the airfoil. Compared to Fig. 6b, these two vortices are not symmetric. Compared to Fig. 7b, the upper vortex is closer to the airfoil and larger in magnitude.

53
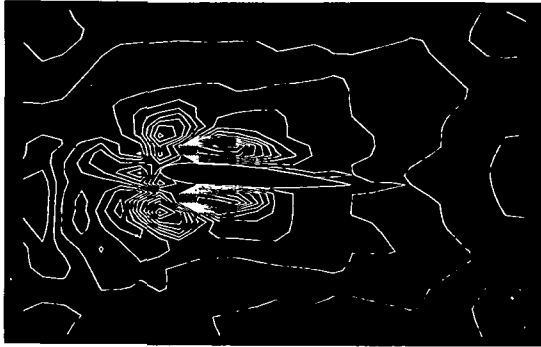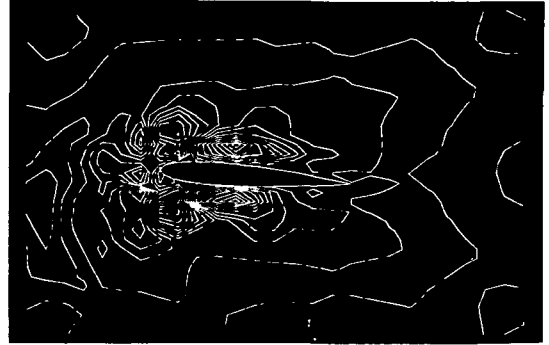
t = 0.104 sec.                          t = 0.112 sec.
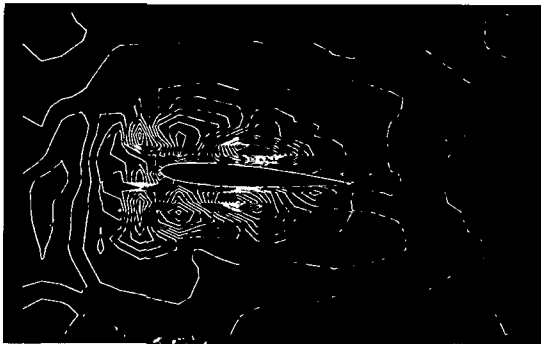
t = 0.120 sec.                          t = 0.128 sec.
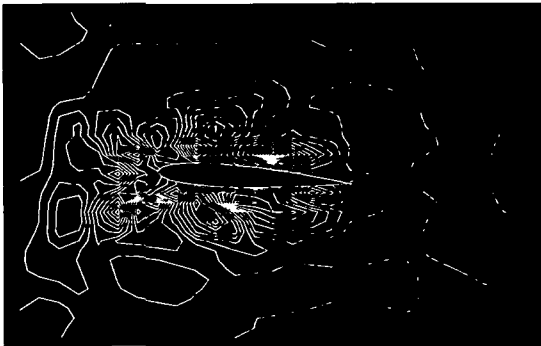
t = 0.136 sec.                          t = 0.144 sec.
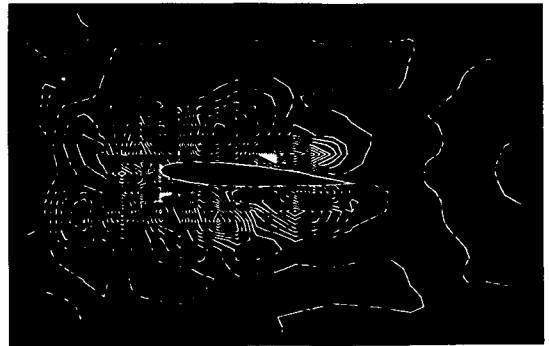
Fig. 8c. Vorticity distribution around a NACA 0012 airfoil.
(Re = $10^5$, $\alpha$ = 4°). The vorticity distribution around the
airfoil reaches a steady state. Compared to Fig. 7c, the
vortices are much closer to the airfoil and exhibit an
unsteady behavior at the leading edge.
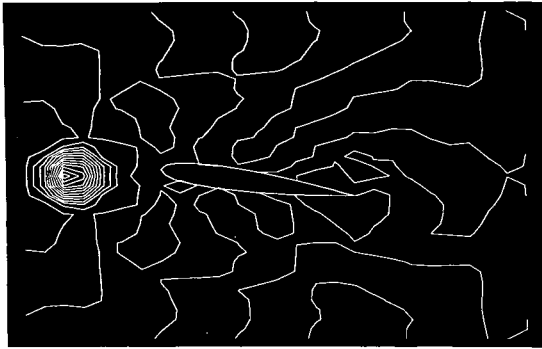
t = 0.1 sec.
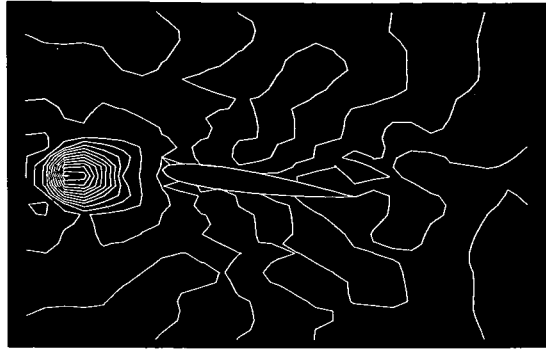
t = 0.8 sec.
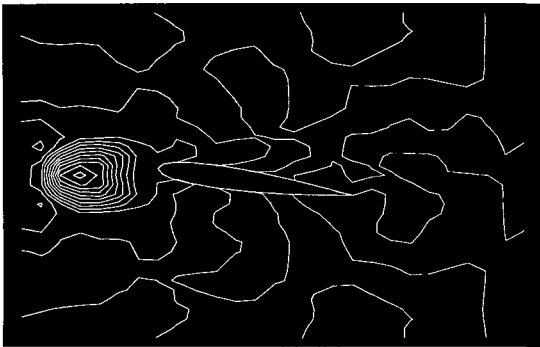
t = 1.6 sec.
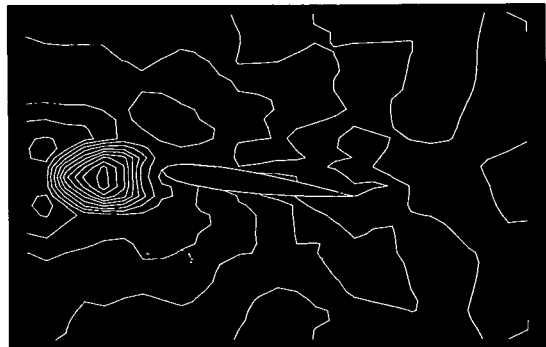
t = 2.4 sec.
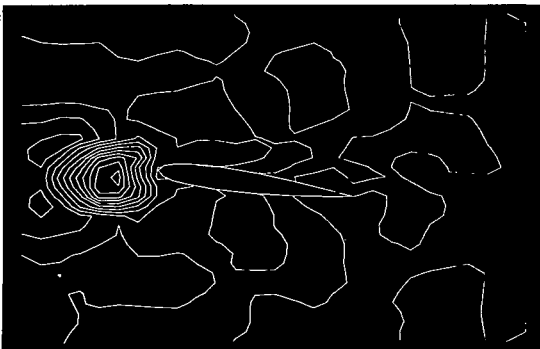
t = 3.2 sec.
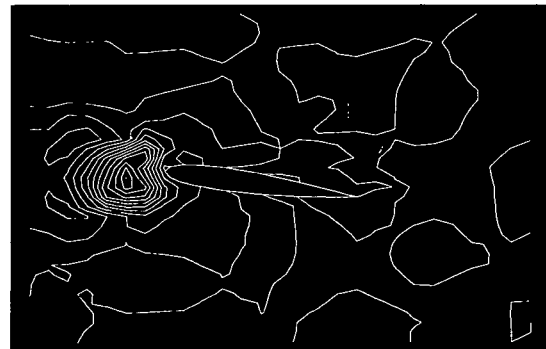
t = 4.0 sec.

Fig. 9a. Vorticity distribution around a NACA 0012 airfoil. (Re = $10^3$, $\alpha$ = 8°). A unit vortex, starting from the same position as in Fig. 5a and 7a, approaches the airfoil.
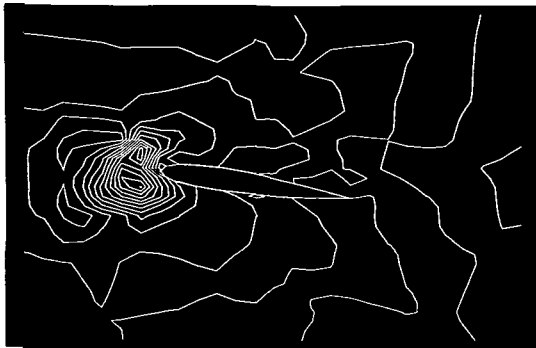
t = 4.8 sec.
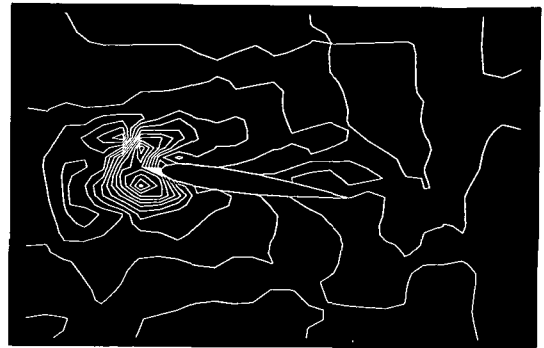
t = 5.6 sec.
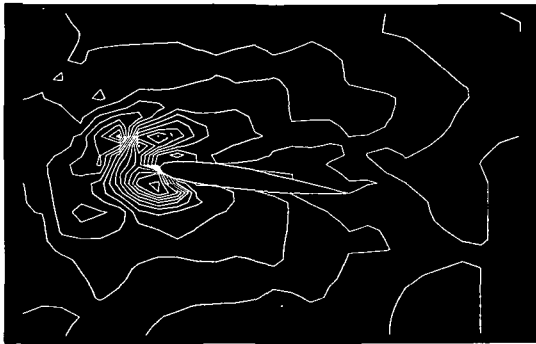
t = 6.4 sec.
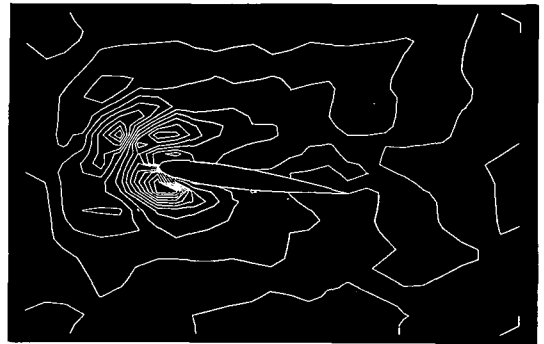
t = 7.2 sec.
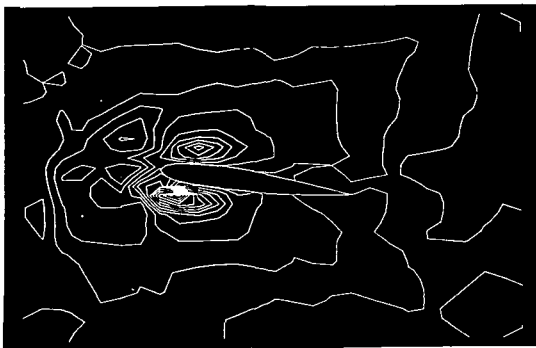
t = 8.0 sec.
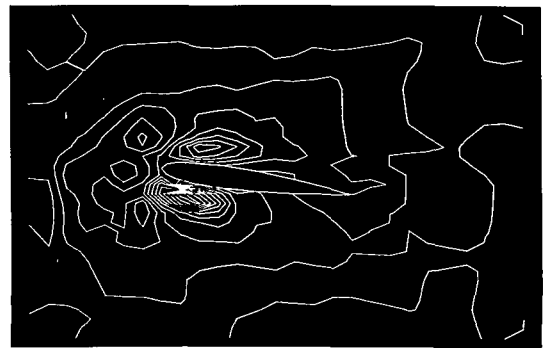
t = 8.8 sec.

Fig. 9b. Vorticity distribution around a NACA 0012 airfoil. (Re = $10^3$, $\alpha$ = 8°). The vortex strikes the airfoil and separates into two vortices. Compared to conditions shown in Fig. 7b, the upper vortex remains closer to the airfoil.
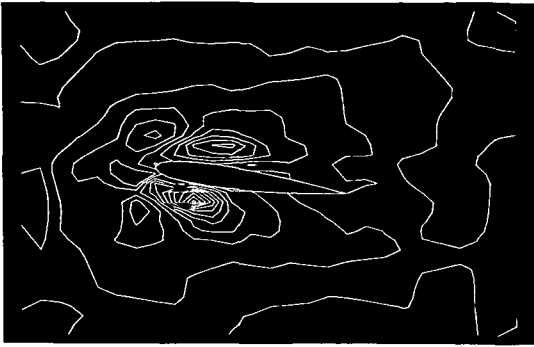
t = 9.6 sec.
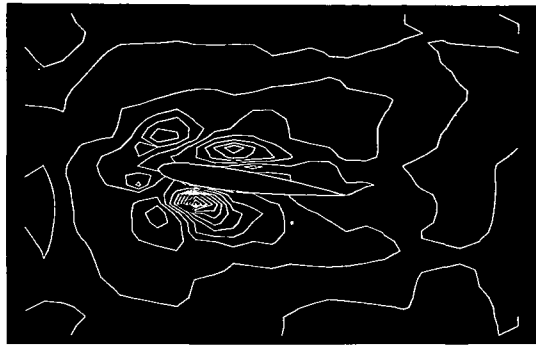
t = 10.4 sec.
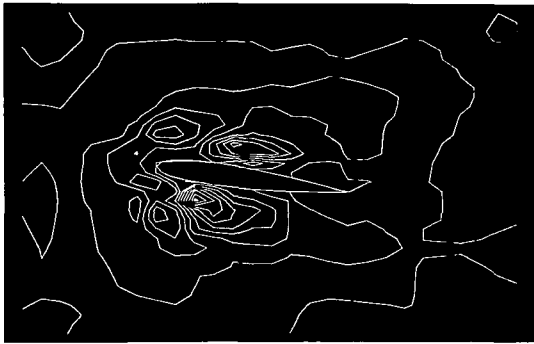
t = 11.2 sec.
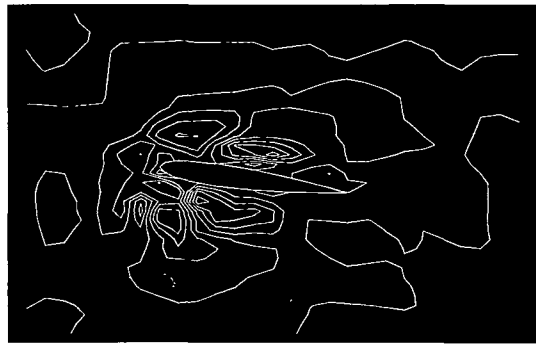
t = 12.0 sec.

t = 12.8 sec.
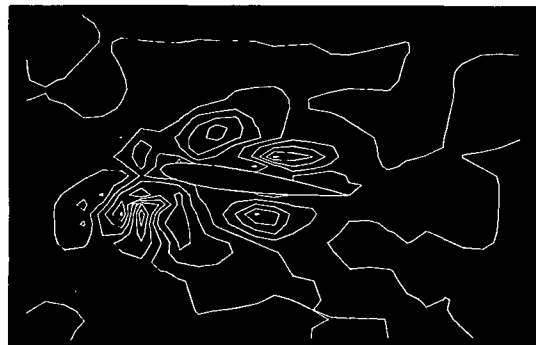
t = 13.6 sec.

Fig. 9c. Vorticity distribution around a NACA 0012 airfoil. (Re = $10^3$, $\alpha = 8°$). The vortices advance along the blade and reach a steady state at almost the same time as the case shown in Fig. 7c. The vortex generated in the unsteady region at the leading edge of the airfoil, as seen in Fig. 5c and 7c, moves along the lower edge in this case.
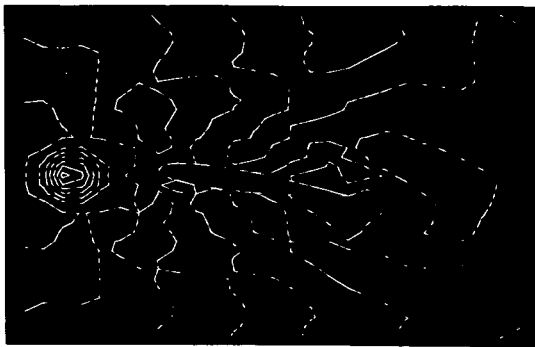
t = 0.002 sec.
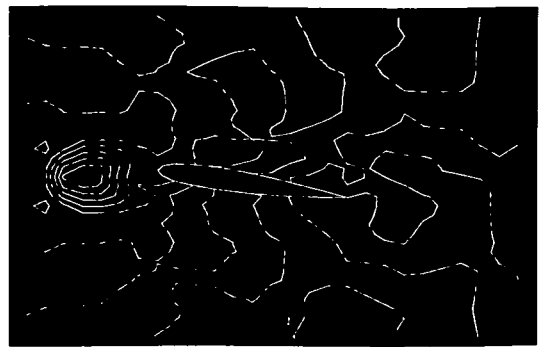
t = 0.016 sec.

t = 0.032 sec.
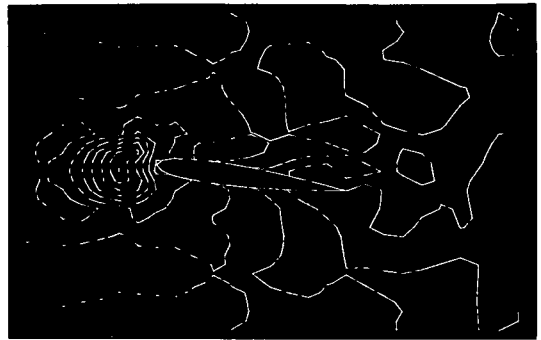
t = 0.040 sec.
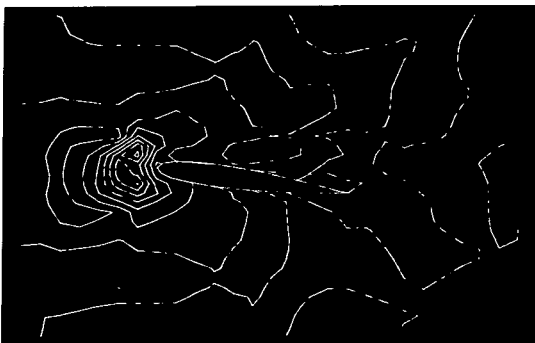
t = 0.048 sec.

t = 0.056 sec.

Fig. 10a. Vorticity distribution around a NACA 0012 airfoil.
(Re = $10^5$, $\alpha = 8°$). A unit vortex, starting from the same
position as in Fig. 6a and 8a, approaches the airfoil.

t = 0.064 sec.

t = 0.072 sec.
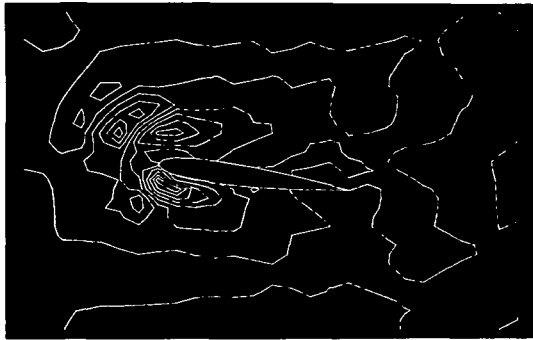
t = 0.080 sec.
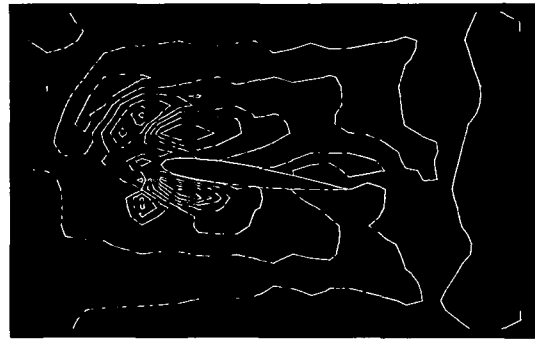
t = 0.088 sec.
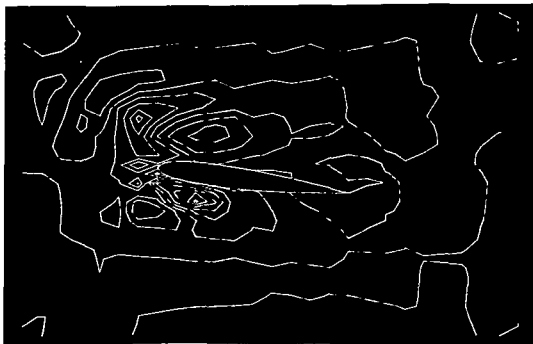
t = 0.096 sec.
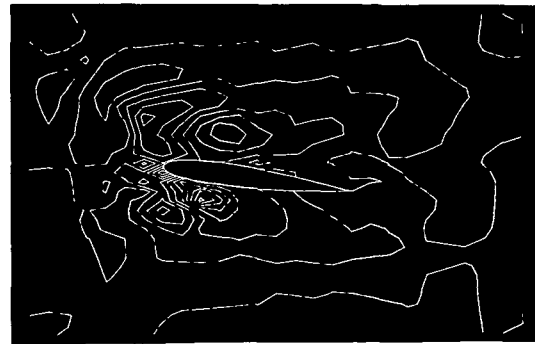
t = 0.104 sec.

Fig. 10b. Vorticity distribution around a NACA 0012 airfoil. (Re = $10^5$, $\alpha$ = 8°). The vorticity distribution at the leading edge of the airfoil is increased.
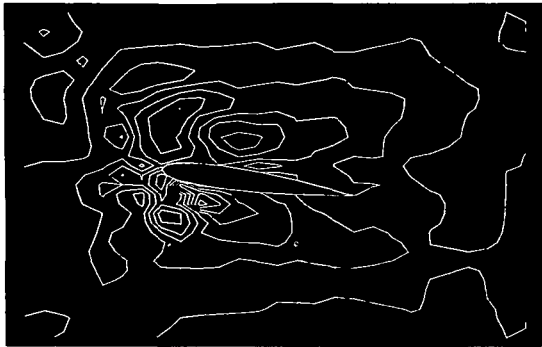
t = 0.112 sec.
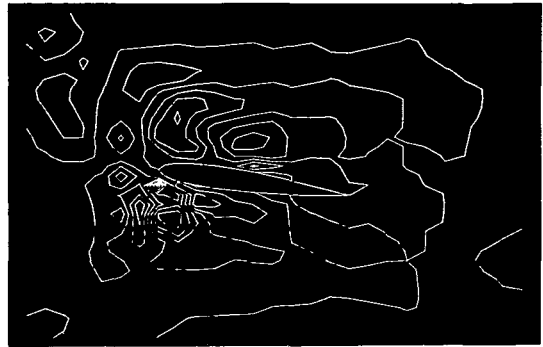
t = 0.120 sec.
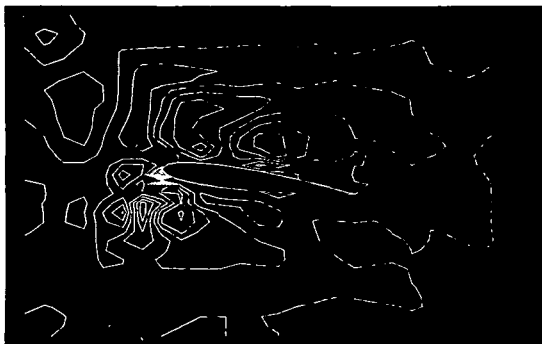
t = 0.128 sec.
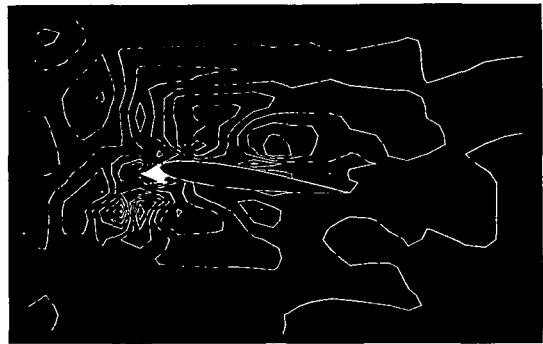
t = 0.136 sec.

t = 0.144 sec.
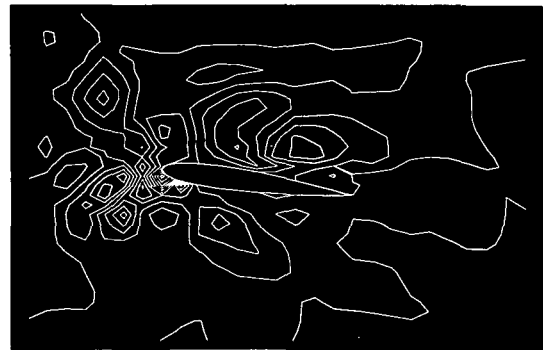
t = 0.152 sec.

Fig. 10c. Vorticity distribution around a NACA 0012 airfoil.
(Re = $10^5$, $\alpha$ = 8°). Steady state is obtained along the airfoil.
Compared to Fig. 9c, the upper vortex is nearer to the trailing
edge, while the lower vortex is lagging. The vorticity
distribution is increased at the leading edge.
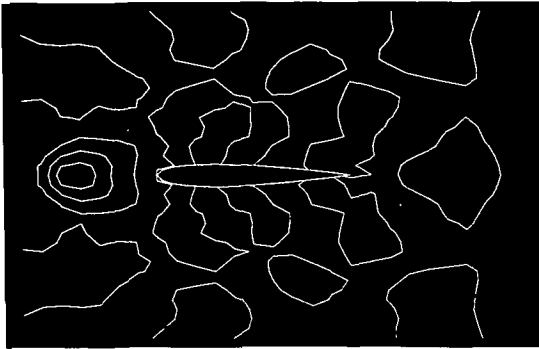
t = 0.012 sec.
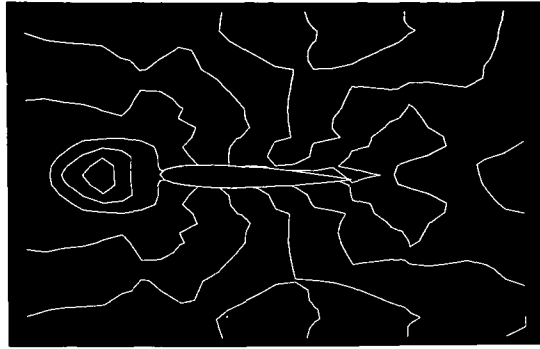
t = 0.024 sec.
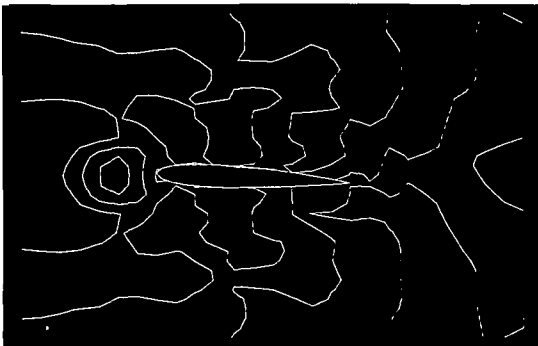
t = 0.036 sec.
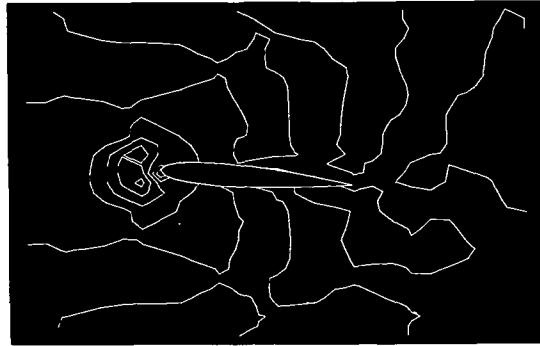
t = 0.048 sec.
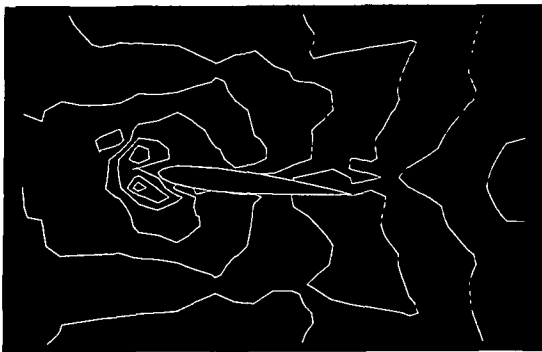
t = 0.060 sec.
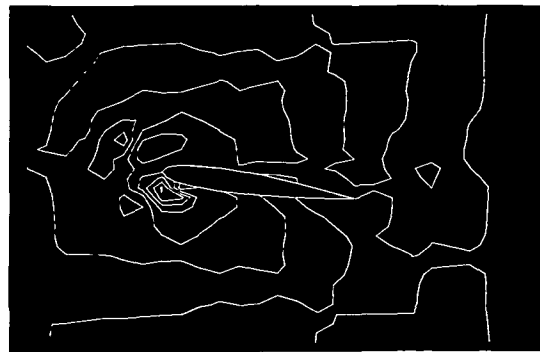
t = 0.072 sec.

Fig. 11a. Vorticity distribution around a pitching NACA 0012 airfoil. (Re = $10^5$). The airfoil is pitching upwards starting from a horizontal position. The initial vortex has the same magnitude as in the previous cases, however, the vorticity distribution was plotted using a larger scale.
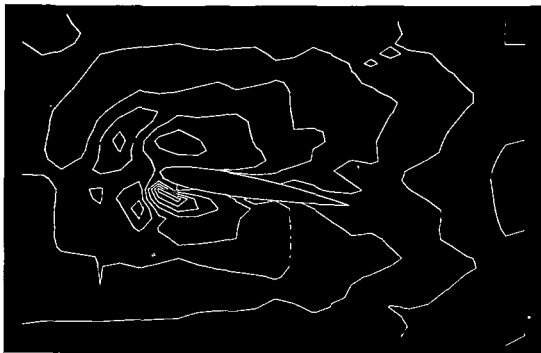
t = 0.084 sec.
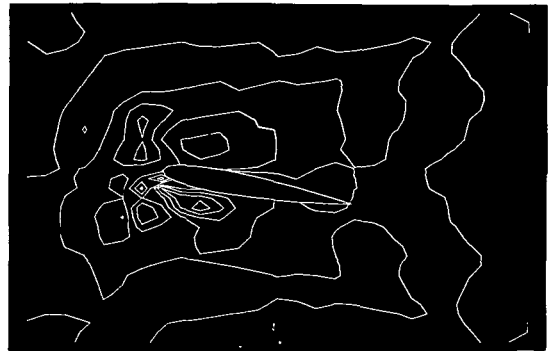
t = 0.096 sec.

t = 0.108 sec.
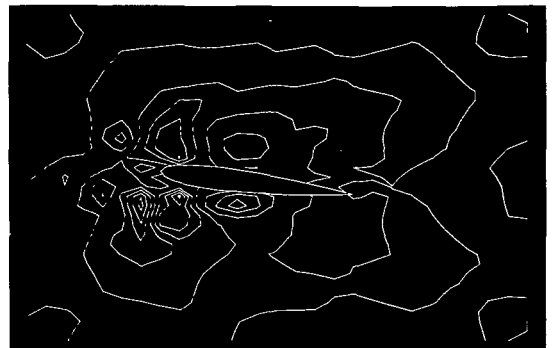
t = 0.120 sec.

t = 0.132 sec.
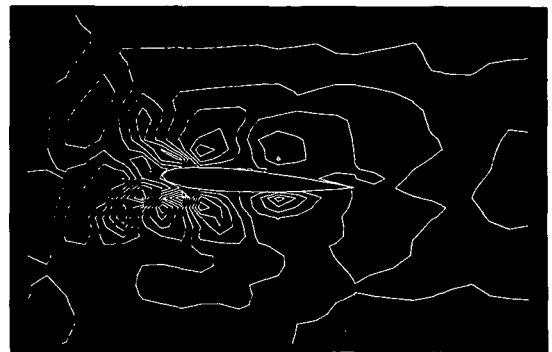
t = 0.144 sec.

Fig. 11b. Vorticity distribution around a pitching NACA 0012 airfoil. (Re = $10^5$). As the vortex strikes the airfoil a series of vortices are generated. These vortices travel along the blade in a similar fashion to the ones in Fig. 10b.
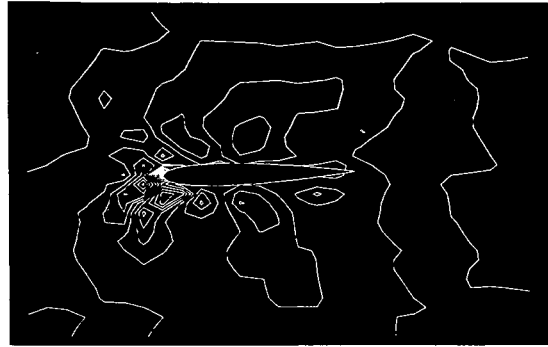
t = 0.156 sec.                    t = 0.168 sec.
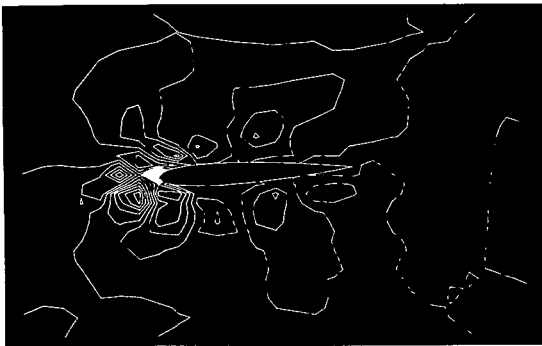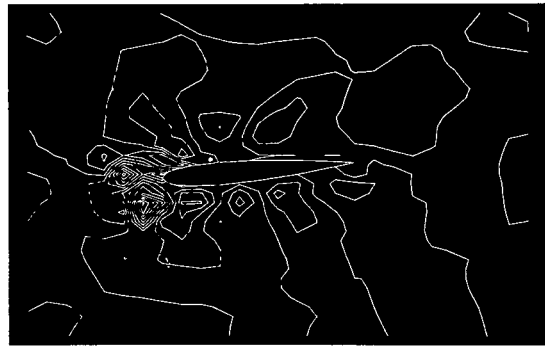
t = 0.180 sec.                    t = 0.192 sec.
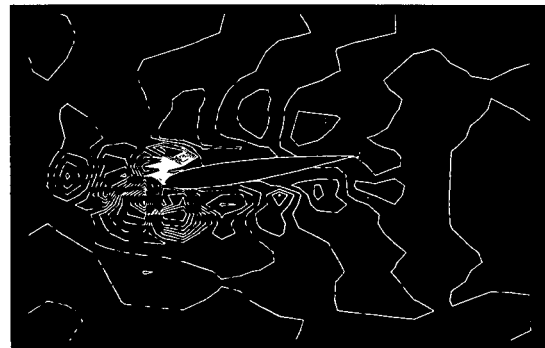
t = 0.204 sec.                    t = 0.216 sec.

Fig. 11c.   Vorticity distribution around a pitching NACA 0012
airfoil.   (Re = $10^5$).   The numerical integration of the vorticity
transport equations was advanced in time for the case shown in
Fig. 11a and 11b.   The vorticity distribution was plotted using
a larger scale.   As the blade continues pitching, new vortices
are generated at the leading edge of the blade.
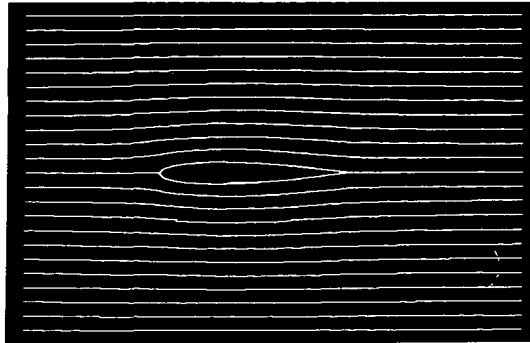
$\alpha = 0°$, Re = $10^5$, t = 0.144 sec.
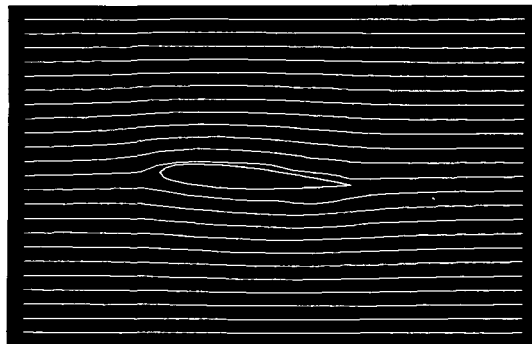


$\alpha = 4°$, Re = $10^5$, t = 0.122 sec.
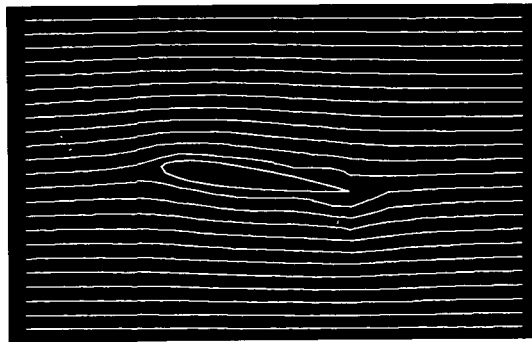


$\alpha = 8°$, Re = $10^5$, t = 0.128 sec.

Fig. 12.  Streamlines around a NACA 0012 airfoil.  The
streamlines were plotted from values of streamfunctions at
each step of the numerical integration of the vorticity
transport equations.  For the sample cases shown in
Fig. 5 - 1, streamlines are illustrated above at several
time increments.
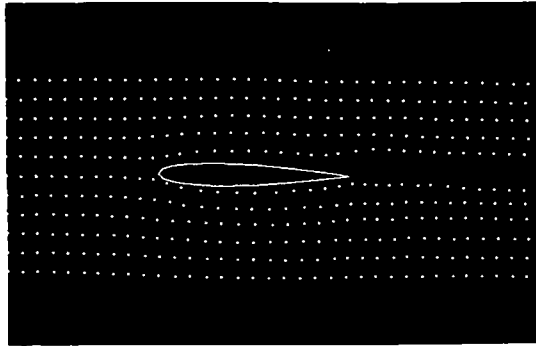
$\alpha = 0°$, Re = $10^5$, t = 0.05 sec.
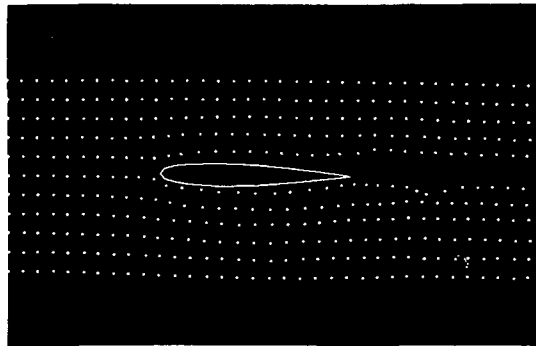


$\alpha = 0°$, Re = $10^5$, t = 0.07 sec.
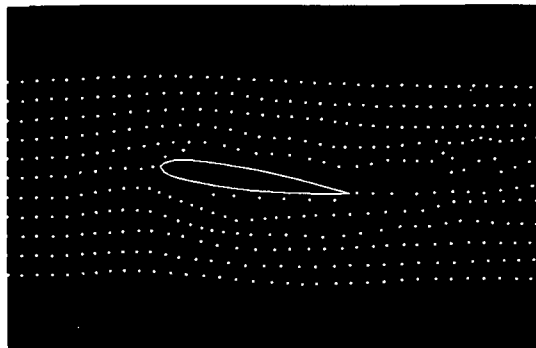


$\alpha = 8°$, Re = $10^5$, t = 0.05 sec.

Fig. 13.  Streaklines around a NACA 0012 airfoil.  The velocity
distribution around the airfoil was obtained from the solution
of vorticity transport equations, as a function of time.  The
positions of a series of air particles were calculated by
numerical integration, the position of several particles
which started from the same points were plotted.

65
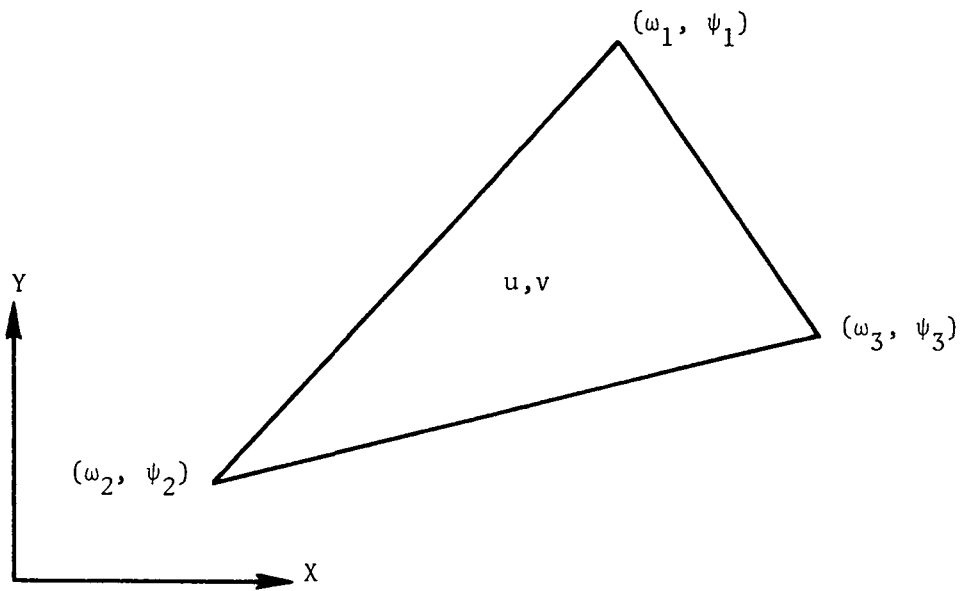
Fig. 14.  A typical triangular grid element for the finite
element analysis of potential flow
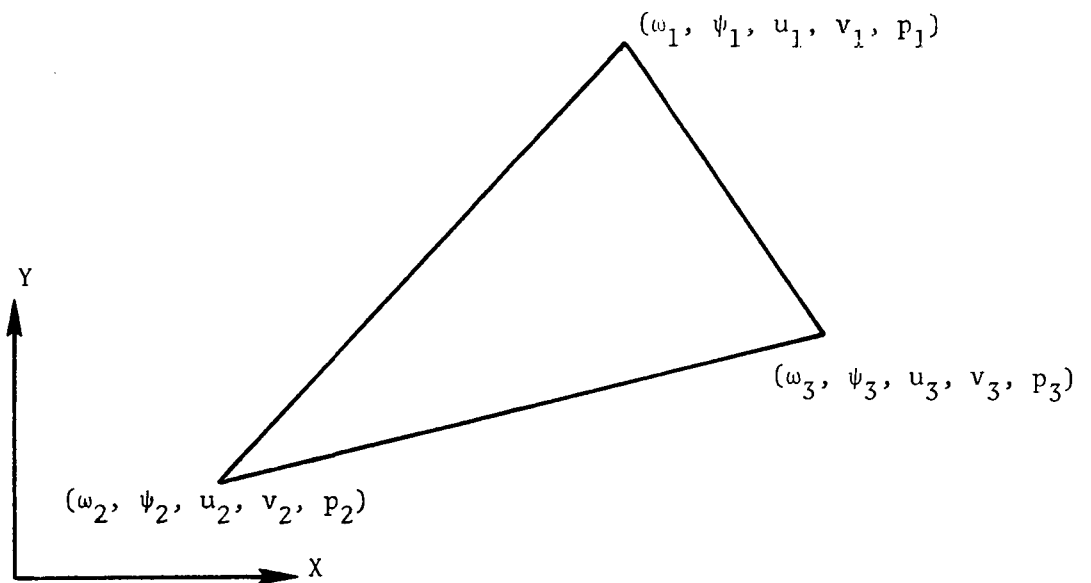


Fig. 15.  A typical triangular grid element for the finite
element analysis of Navier-Stokes equations

66
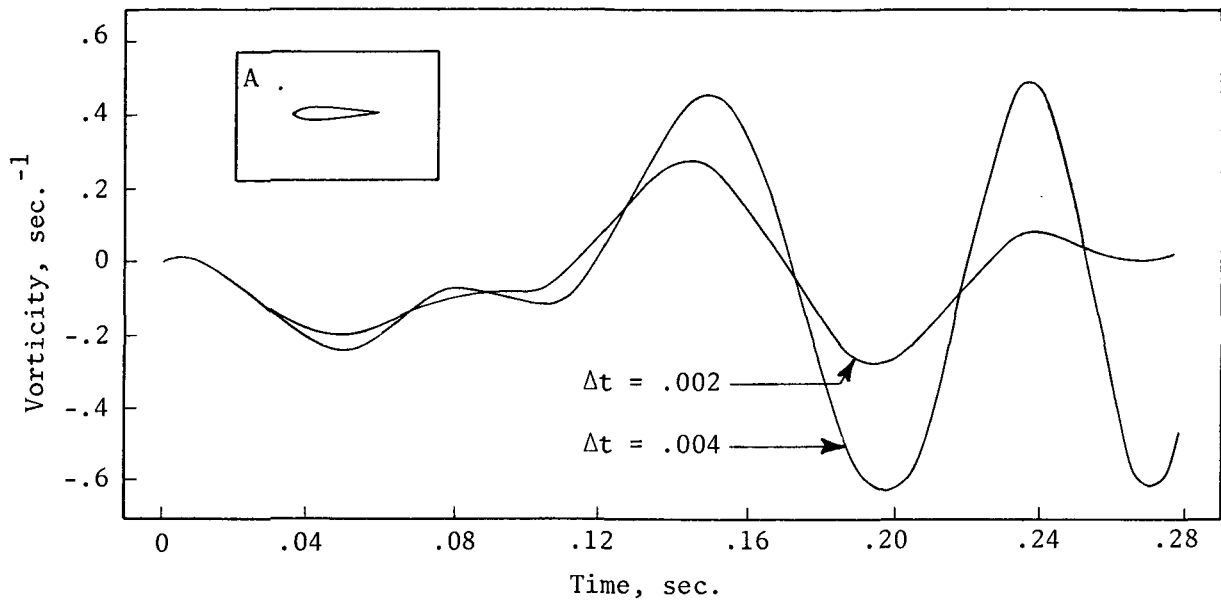
Fig. 16a. Accuracy and stability of numerical integration of the vorticity transport equation for a point (A) upstream of the airfoil. ($\alpha$ = 0, Re = $10^5$).
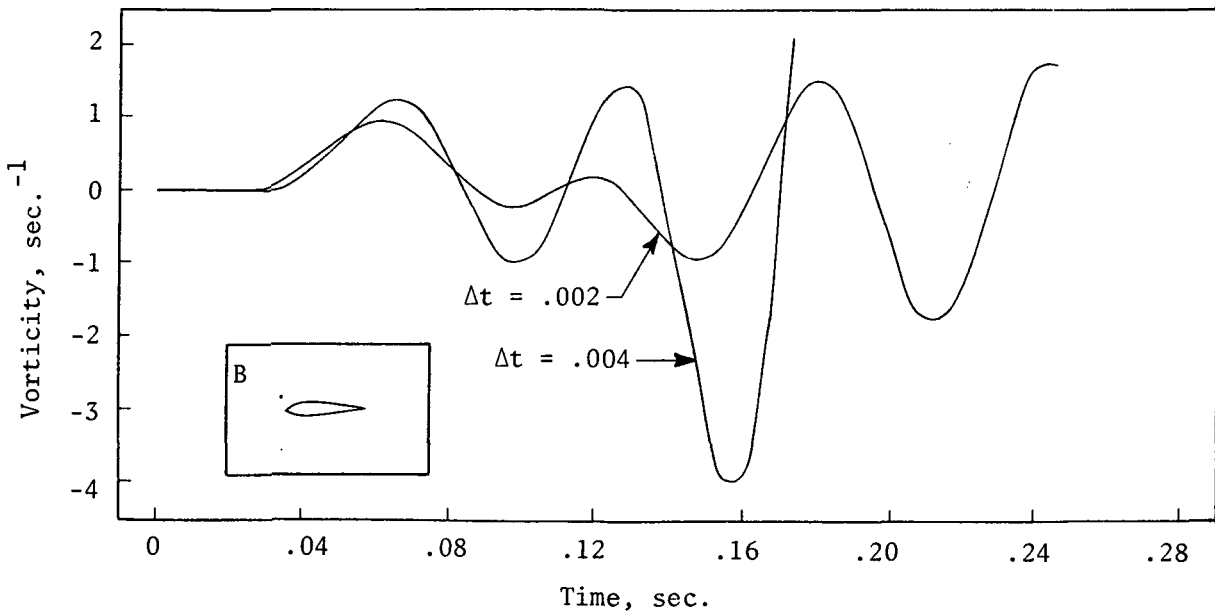


Fig. 16b. Accuracy and stability of numerical integration of the vorticity transport equation for a point (B) in the vicinity of the airfoil. ($\alpha$ = 0, Re = $10^5$).